Statistical characteristics of two-dimensional and quasigeostrophic turbulence

by

Andreas Vallgren

June 2010
Technical Reports
Royal Institute of Technology
Department of Mechanics
SE-100 44 Stockholm, Sweden

Akademisk avhandling som med tillstånd av Kungliga Tekniska Högskolan i Stockholm framlägges till offentlig granskning för avläggande av filosofie licentiatsexamen måndagen den 14 juni 2010 kl 10.15 i sal E2, Kungliga Tekniska Högskolan, Lindstedtsvägen 3, Stockholm.

©Andreas Vallgren 2010

Universitetsservice US-AB, Stockholm 2010

Statistical characteristics of two-dimensional and quasigeostrophic turbulence

Andreas Vallgren

Linné Flow Centre, Department of Mechanics, Royal Institute of Technology (KTH)

SE-100 44 Stockholm, Sweden

Abstract

Two codes have been developed and implemented for use on massively parallel super computers to simulate two-dimensional and quasigeostrophic turbulence. The codes have been found to scale well with increasing resolution and width of the simulations. This has allowed for the highest resolution simulations of twodimensional and quasigeostrophic turbulence so far reported in the literature. The direct numerical simulations have focused on the statistical characteristics of turbulent cascades of energy and enstrophy, the role of coherent vortices and departures from universal scaling laws, theoretized more than 40 years ago. In particular, the investigations have concerned the enstrophy and energy cascade in forced and decaying two-dimensional turbulence. Furthermore, the applicability of Charnev's hypotheses on quasigeostrophic turbulence has been tested. The results have shed light on the flow evolution at very large Reynolds numbers. The most important results are the robustness of the enstrophy cascade in forced and decaying two-dimensional turbulence, the unexpected dependency on an infrared Reynolds number in the spectral scaling of the energy spectrum in the inverse energy cascade, and the validation of Charney's predictions on the dynamics of quasigeostrophic turbulence. It has also been shown that the scaling of the energy spectrum in the enstrophy cascade is insensitive to intermittency in higher order statistics, but that corrections might apply to the "universal" Batchelor-Kraichnan constant.

Descriptors: two-dimensional turbulence, decaying turbulence, quasigeostrophic turbulence, direct numerical simulation (DNS), coherent vortices, energy cascade, enstrophy cascade, intermittency, massively parallel simulations

Preface

This thesis investigates the statistical characteristics of two-dimensional and quasigeostrophic turbulence, by high resolution direct numerical simulations. The first part introduces some fundamental concepts in the understanding of the two turbulent regimes and links these to current research activities. The second part is a collection of the following articles:

Paper 1. A. VALLGREN & E. LINDBORG,

The enstrophy cascade in forced two-dimensional turbulence. Under consideration for publication in the Journal of Fluid Mechanics.

Paper 2. E. LINDBORG, A. VALLGREN & P. DAVIDSON,

Testing Batchelor's similarity hypotheses for decaying two-dimensional turbulence. Submitted to Physical Review Letters.

Paper 3. A. VALLGREN,

Infrared Reynolds number dependency of the two-dimensional inverse energy cascade. Submitted to the Journal of Fluid Mechanics.

Paper 4. A. VALLGREN & E. LINDBORG,

Charney isotropy and equipartition in quasigeostrophic turbulence Accepted for publication in the Journal of Fluid Mechanics.

Paper 5. A. VALLGREN,

 $Simulations\ of\ two-dimensional\ and\ quasige ostrophic\ turbulence$ Technical Report.

Division of work between authors

The research project was initiated by Dr. Erik Lindborg (EL) who has been the main supervisor. Dr. Geert Brethouwer (GB) was co-advisor. Prof. Peter Davidson (PD) was collaborator.

Paper 1

The code was developed and implemented by Andreas Vallgren (AV), in collaboration with EL and GB. Simulations were performed by AV. Most of the paper was written by AV with input from EL. EL wrote the introduction.

Paper 2

The simulations were performed by AV. The paper was written by EL, with input from AV and PD. PD initiated a discussion on decaying two-dimensional turbulence based on recent findings during a visit to the Linné FLOW centre, which instigated the numerical study.

Paper 3

The simulations were performed by AV. The paper was written by AV.

Paper 4

The code was developed and implemented by AV, in collaboration with EL. The simulations were performed by AV, who also wrote the paper with input from EL.

Paper 5

The technical report was written by AV.

V



Contents

Abstract	iii			
Preface	iv			
Part I - Introduction				
Chapter 1. Introduction	1			
Chapter 2. Strictly two-dimensional turbulence	5			
2.1. Introduction	5			
2.2. The enstrophy cascade	8			
2.3. The energy cascade	10			
2.4. Decaying turbulence	11			
2.5. Coherent structures	12			
2.6. β -plane turbulence	13			
Chapter 3. Quasigeostrophic turbulence	16			
Chapter 4. Numerical method and the codes	18			
Chapter 5. Summary of the papers	19			
Paper 1	19			
Paper 2	19			
Paper 3				
Paper 4				
Paper 5	20			
Chapter 6. Outlook	21			
Acknowledgements	22			
Appendix A. Derivation of the QG potential				
vorticity equation	23			
A.1. Introduction	23			
A.2. Scaling the 3D Navier-Stokes equation	23			
A.3. The geostrophic approximation	28			
A.4. Using static stability to resolve the vertical motion	32			
A.5. The quasigeostrophic potential vorticity equation	34			

A.6. Connecting the QGPV equation to Charney's theory A.7. The role of the β -term			
Bibliograpl	ny	46	
	Part II - Papers		
Paper 1.	The enstrophy cascade in forced two-dimensional turbulence	53	
Paper 2.	Testing Batchelor's similarity hypotheses for decaying two-dimensional turbulence	73	
Paper 3.	Infrared Reynolds number dependency of the two-dimensional inverse energy cascade	83	
Paper 4.	Charney isotropy and equipartition in quasigeostrophic turbulence	97	
Paper 5.	Simulations of two-dimensional and quasigeostrophic turbulence	111	

Part I Introduction

CHAPTER 1

Introduction

Welcome to the amazing Flatlands! A very conservative place where only viscosity makes a difference and where new ideas are often abandoned in favour of the original predictions. The statistical properties of two-dimensional turbulence are still, 40 years from when it was more profoundly theoretized, an active research field. Despite the apparent simplicity in dealing with two rather than three spatial dimensions, 2D turbulence is possibly richer in its dynamics than 3D turbulence. The reason is found in its conservational properties. Both energy and a multitude of vorticity quantities, called Casimirs, are inviscidly conserved, the latter on a parcel. One such Casimir, enstrophy, defined as $\Omega = \omega^2/2$ where $\omega = \mathbf{e}_z \cdot \nabla \times \mathbf{u}$ is the vorticity and \mathbf{u} is the two-dimensional velocity field, has profound importance in two-dimensional turbulence, as we will see. The conserved quantities impose restrictions on the flow evolution and is thus of both mathematical and physical interest. Perhaps of most physical relevance, is the observation that there is no forward energy cascade as in three-dimensional turbulence. Richardson's (1922) view of 3D turbulence was summarized as

> Big whorls have little whorls, Which feed on their velocity; And little whorls have lesser whorls, And so on to viscosity.

In two-dimensional turbulence, this picture is reversed, with energy cascading towards larger scales, while enstrophy cascades towards smaller scales. One might then ask why we care about two-dimensional turbulence, seemingly just an academic topic very far from the real world? A few moments thought reveals that it might not be just of academic interest. We may find quasi-two-dimensional flows in a wide variety of situations. One such example is the flow in a fluid film on top of a surface of another fluid or a rigid object. Another example is a rapidly rotating fluid. A third example, which is the main motivation of this thesis, is the approximate 2D nature of tropospheric and oceanic flows (see figure 1.1, illustrating typical flow structures). This can be understood as a consequence of the small aspect ratio D/L of large scale flow structures, where $D \sim 10$ km is the approximate scale height of the troposphere and $L \sim 1000$ km is the typical length scale of cyclones and anticyclones, advected by a practically horizontal flow. In fact, the motion of tropical cyclones have

1

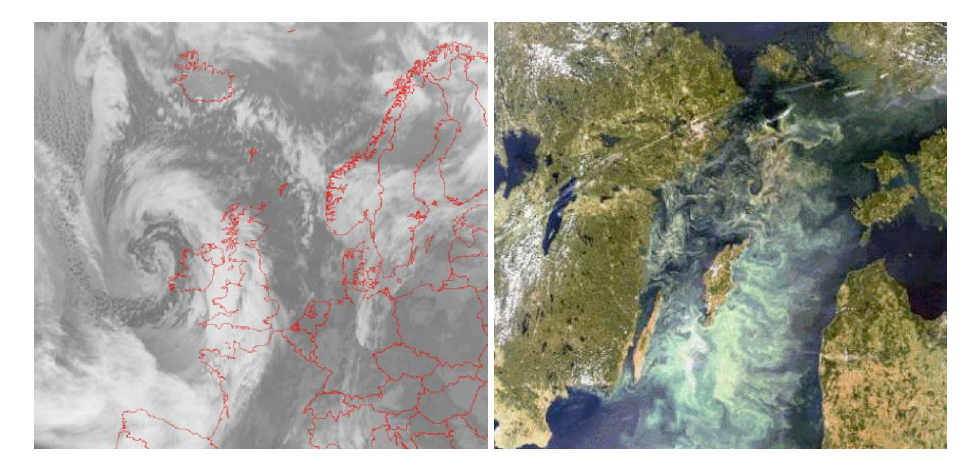


FIGURE 1.1. Examples of quasi-2D flow regimes. Left: Infrared satellite image from March 10, 2008, showing a mature cyclone west of the British Isles. Right: RGB satellite image showing an algal bloom event in the Baltic Sea, acting as a passive tracer showing the flow field near the sea surface. From SMHI.

been successfully predicted by 2D vortex models (Tabeling, 2002). The question is whether the atmospheric (kinetic) energy spectrum can be explained by two-dimensional turbulence. Nastrom and Gage (1985) and Gage and Nastrom (1986) presented observational data on the energy spectrum, showing a k^{-3} kinetic energy spectrum at large scales and a $k^{-5/3}$ -spectrum at scales smaller than about 500 km (see figure 1.2). There have been numerous attempts to explain these observations in terms of 2D turbulence over the years, e.g., Lilly (1983), Smith and Yakhot (1994) and Tung and Orlando (2003). Lindborg (1999; 2006) argued that the k^{-3} -range can be explained in terms of a 2D enstrophy inertial range whereas the $k^{-5/3}$ -range should most likely not be interpreted as a result of 2D turbulent interactions. Thus, although there is much evidence for a 2D enstrophy cascade range at large scales, the dynamical origin of the $k^{-5/3}$ -range at high wave numbers is still debated. There are namely two possible candidates for such a range; a forward cascade of 3D turbulent energy (e.g., Lindborg, 2006 and Tung and Orlando, 2003) or an inverse cascade of 2D energy (e.g., Lilly, 1983; Smith, 2004). The former depends on energy being fed from large-scale baroclinic motions and the latter from convective sources such as thunderstorms. To settle this question, one needs to increase the complexity in the modeling by allowing for rotation and stratification, which are two important features of tropospheric flow. Charney (1971) derived a theory of what is called quasigeostrophic turbulence. This turbulent regime takes into account the effect of background rotation and a stable stratification, and describes the flow dynamics at relatively large, synoptic, scales. A key point in Charney's theory was the introduction of a stretched coordinate in the vertical,

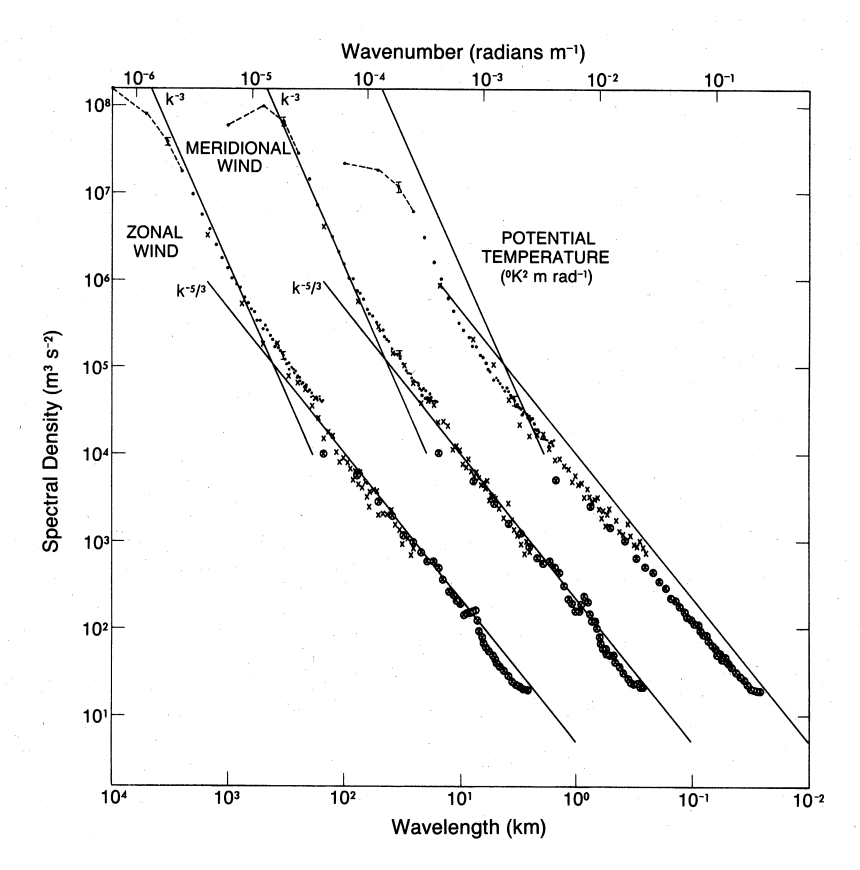


FIGURE 1.2. Observed kinetic energy spectrum divided into zonal and meridional components and potential energy spectrum in terms of the potential temperature, clearly indicating the existence of two spectral ranges. From Nastrom and Gage (1985).

 $\zeta=(N/f)z$, where N is the Brunt-Väisälä frequency which is a measure of the stratification and f is the Coriolis parameter which is a measure of the rotation rate. By doing this, Charney predicted a clear analogy with two-dimensional turbulence, in terms of cascade directions and approximately isotropic and homogeneous energy spectra. This thesis explores the statistical characteristics of pure two-dimensional and quasigeostrophic turbulence in order to approach the subtle question about the origins of the atmospheric energy spectrum. This has been accomplished by developing two codes by which a number of direct numerical simulations have been carried out for these two flow regimes. Not only is the nature of large-scale atmospheric turbulence interesting in its own right, but the outcomes of these studies are also of interest for the development of operational forecast and climate models. The next sections will describe the

4 1. INTRODUCTION

statistical characteristics of two-dimensional and quasigeostrophic turbulence in more detail. For a more thorough review of two-dimensional turbulence, the reader is referred to Tabeling (2002) and Danilov and Gurarie (2000). The latter authors also cover quasi-2D turbulence including quasigeostrophic turbulence.

CHAPTER 2

Strictly two-dimensional turbulence

2.1. Introduction

Richardson's view of the turbulent cascade cannot be valid in two-dimensional turbulence. The physical constraints imposed on a two-dimensional flow, prevent a dominant forward energy cascade. The constraints follow from inviscid conservation of both energy and enstrophy, which can be realized by deriving the energy and enstrophy equation resulting from multiplying the 2D Navier-Stokes equation by ${\bf u}$ and the vorticity equation by ω , respectively. The incompressible Navier-Stokes equation in its vorticity formulation is given by

$$\frac{\partial \omega}{\partial t} + (\boldsymbol{u} \cdot \nabla)\omega = \nu \nabla^2 \omega, \tag{2.1}$$

where ν is the kinematic viscosity. One way to picture the role of the inviscid ($\nu = 0$) conservation properties is to consider the temporal evolution of the energy and enstrophy centroid wave numbers, respectively, following Vallis (2006). Noting that the mean energy and enstrophy can be written as

$$\bar{E} = \frac{1}{2} \int \left(u^2 + v^2 \right) dA = \frac{1}{2} \int \left[\left(\frac{\partial \psi}{\partial y} \right)^2 + \left(\frac{\partial \psi}{\partial x} \right)^2 \right] dA, \tag{2.2}$$

$$\bar{\Omega} = \frac{1}{2} \int \omega^2 dA = \frac{1}{2} \int \left(\nabla^2 \psi\right)^2 dA, \tag{2.3}$$

where $\omega = \mathbf{e}_z \cdot \nabla \times \mathbf{u}$ is the vorticity and the stream function ψ is defined so that $u = -\partial \psi/\partial y$, $v = -\partial \psi/\partial x$ and $\omega = \nabla^2 \psi$, and transforming into spectral space, we obtain

$$\bar{E} = \int E(k)dk = \frac{1}{2} \int (\widehat{u}\widehat{u}^* + \widehat{v}\widehat{v}^*)dk = -\frac{1}{2} \int k^2 \widehat{\psi}\widehat{\psi}^*dk, \qquad (2.4)$$

$$\bar{\Omega} = \int \Omega(k)dk = \frac{1}{2} \int \widehat{\omega}\widehat{\omega}^* dk = -\frac{1}{2} \int k^4 \widehat{\psi}\widehat{\psi}^* dk = \int k^2 E(k)dk.$$
 (2.5)

We now define the energy centroid wave number as

$$k_E = \frac{\int kE(k)dk}{\int E(k)dk},\tag{2.6}$$

and introduce

$$I = \int (k - k_E)^2 E(k) dk = \int k^2 E(k) dk - k_E^2 \int E(k) dk,$$
 (2.7)

which upon temporal differentiation gives a measure of the spreading of the energy distribution. To obtain (2.7), the definition of k_E (2.6) has been used. If all energy is initially centred at k_E , dI/dt should be larger than zero. Since both energy and enstrophy are inviscibly conserved, it follows that

$$\frac{dk_E}{dt} = -\frac{1}{2k_E\bar{E}}\frac{dI}{dt} < 0, \tag{2.8}$$

(2.9)

which is consistent with an inverse energy cascade, i.e., a transfer of energy towards larger scales. Similarly, if we introduce an enstrophy wave number centroid k_{Ω} and let

$$k_{\Omega} = \frac{\int \Omega(k)dk}{\int k^{-1}\Omega(k)dk},$$
(2.10)

and introduce

$$J = \int (k^{-1} - k_{\Omega}^{-1})^2 \Omega(k) dk = \int E(k) dk - k_{\Omega}^{-2} \int \Omega(k) dk, \qquad (2.11)$$

a little manipulation yields

$$\frac{dk_{\Omega}}{dt} = \frac{k_{\Omega}^3}{2\bar{\Omega}} \frac{dJ}{dt} > 0. \tag{2.12}$$

Thus, the enstrophy wave number centroid (in which all enstrophy is initially located) moves towards higher wave numbers (smaller scales) with time, which can be interpreted as a forward cascade of enstrophy. These are heuristic arguments but nevertheless show the general tendency for the cascade directions. Note that this argument does not forbid energy to be transferred to smaller scales, it just tells that more of the energy propagates towards larger scales. The same argument holds for the enstrophy cascade.

Our next step is to elaborate on the existence of a double cascade scenario and inertial ranges in two-dimensional turbulence. Let us consider a case in which we feed a turbulent system with energy at a scale k_f . Given that the general picture of the cascade directions holds, as reflected by the time evolution of wave number centroids, we would expect energy to propagate upscale and enstrophy to propagate downscale. If there is no large-scale drag imposed and we consider an infinitely large domain, we would expect an undisturbed energy cascade towards larger scales. Simultaneously, we would expect an enstrophy cascade towards smaller scales, ultimately removed by small-scale viscous dissipation. Given a large enough Reynolds number so that $k_f <<$ k_{max} , it is reasonable to expect that there would be a region, $k_f < k < k_{max}$, practically undisturbed by viscous dissipation. Assume that we feed the system with energy at a rate ϵ and enstrophy at a rate η (the two are related by $\epsilon = \eta/k_f^2$). In the energy cascade range, the only parameters of practical importance would be the energy density E(k), the energy injection rate ϵ and wave number k. Accordingly, we let $E(k) \sim \epsilon^a k^b$. Dimensional reasoning gives that a=2/3 and b=-5/3 so that $E(k)\sim\epsilon^{2/3}k^{-5/3}$. Similar argumentation

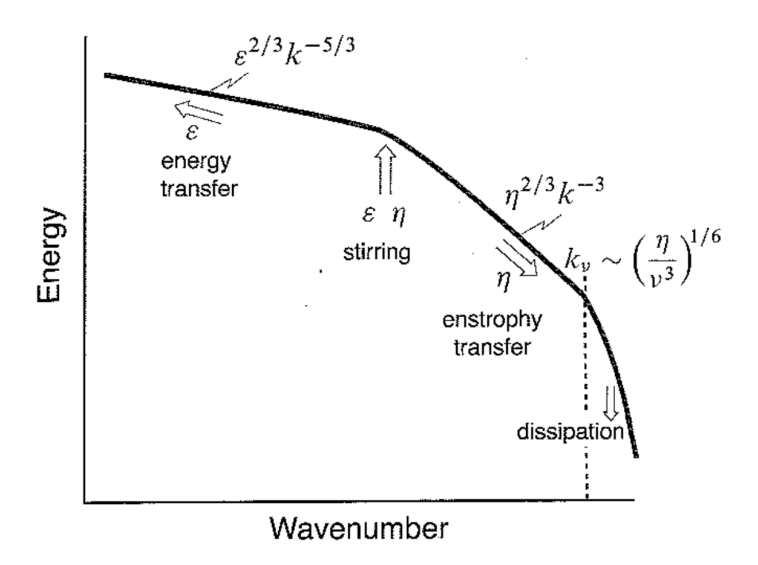


FIGURE 2.1. Qualitative picture of the double cascade of forced two-dimensional turbulence. From Vallis (2006).

gives that $E(k) \sim \eta^{2/3} k^{-3}$ in the forward enstrophy cascade range. These predictions were introduced by Kraichnan (1967) and Leith (1968) and are illustrated in figure 2.1. Thus, for the inverse energy cascade range,

$$E(k) = \mathcal{K}\epsilon^{2/3}k^{-5/3},$$
 (2.13)

and for the enstrophy cascade range;

$$E(k) = C\eta^{2/3}k^{-3}, (2.14)$$

where we refer to \mathcal{C} as the Kraichnan constant in forced two-dimensional turbulence and the Batchelor-Kraichnan constant in decaying two-dimensional turbulence (Batchelor, 1969). One major assumption that these predictions rely on is the locality of the cascades, meaning that it is assumed that there is no interaction with scales outside the inertial ranges. Already in 1967, Kraichnan hypothesized that a logarithmic correction should manifest in the k^{-3} enstrophy cascade range, although he did not provide any exact details on its form. In a follow-up paper, Kraichnan (1971), provided a complimentary theoretical prediction, namely

$$E(k) = C' \eta_{\omega}^{2/3} k^{-3} \left[\ln \left(\frac{k}{k_1} \right) \right]^{-1/3},$$
 (2.15)

where C' is a constant of order unity, which Kraichnan estimated to 2.626 based on a turbulence test-field model and k_1 marks the lowest wavenumber of the inertial range. The reason for this correction to the clean k^{-3} -spectrum, is that the enstrophy flux would otherwise grow with k as a consequence of a diverging

rate of shear integral at low $k \sim k_1$. This correction allows for a k-independent C' and a constant enstrophy flux range.

2.2. The enstrophy cascade

In this section we review the enstrophy cascade in forced two-dimensional turbulence. The cascade theory of Kraichnan (1967) has been tested numerically in a large number of studies, not the least because it is more tractable in terms of computational resources than simulations of the inverse energy cascade. At the time of the early theoretical advances, the computational resources were very limited, but attempts were made to simulate the two-dimensional Navier-Stokes equation. However, the limited resolution available at this time was only enough to indicate a qualitative statistical picture of low Reynolds number 2D turbulence. During the 1980's and 1990's, the computational resources allowed for more resolved and more accurate numerical simulations. The results from these experiments indicated that the k^{-3} or possibly the logarithmically corrected spectrum, was not as robust as anticipated, with reports on steeper energy spectrum (e.g., Legras et al., 1988; Gilbert, 1988; Maltrud and Vallis, 1991, and Kaneda and Ishihara, 2001). The presence of vortices was now believed to distort the spectral shape of the inertial energy spectrum by introducing intermittency. With ever-increasing computational performance, the results once again started to point toward the early theoretical predictions by Kraichnan-Leith (e.g., Lindborg and Alvelius, 2000; Boffetta, 2007 and Bracco and McWilliams, 2010). The logarithmically corrected enstrophy spectrum has been numerically obtained by, e.g., Pasquero and Falkovich, 2002. Most of these studies have included a large-scale friction (also referred to as drag or hypodiffusion) to prevent energy from growing and drive the turbulence into a stationary state where energy is dissipated at large scales at the same rate at which it is injected. If the turbulence is forced at a very small wave number, corresponding to the scale of the computational domain, and no large scale drag is introduced, energy will pile up in the smallest wave numbers and there is a clear risk that a state soon develops which is very different from the double cascade scenario. If the turbulence is forced at a considerably larger wave number, it will become extremely demanding to resolve a sufficiently large span of scales to obtain a broad enstrophy cascade range. Thus, no serious attempt was made to test the perhaps strongest prediction of Kraichnan's theory – the existence of a stationary enstrophy cascade in the absence of large scale drag and in the presence of a constant energy growth. However, we now have performed such simulations. With a series of extremely high resolution simulations, as presented in Paper 1, our results suggest that the enstrophy cascade may indeed be more robust than recently believed. In the absence of a large scale drag, we have obtained results that confirm Kraichnan's original prediction (1967) with a clean k^{-3} energy spectrum in the enstrophy cascade range, without a logarithmic correction, as Kraichnan proposed in his follow-up paper (1971). Figure 2.2 illustrates the real vorticity field in a simulation forced at large scales. Note in particular the dominance of vorticity filaments, indicative

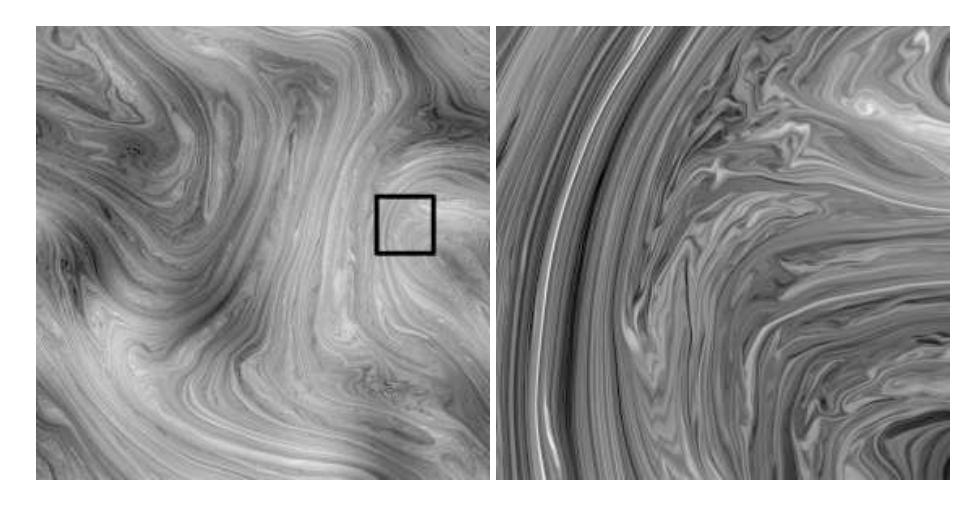


FIGURE 2.2. Vorticity field and zoom in from a simulation forced at large scales, showing the dominance of vorticity filaments, resulting from a forward enstrophy cascade.

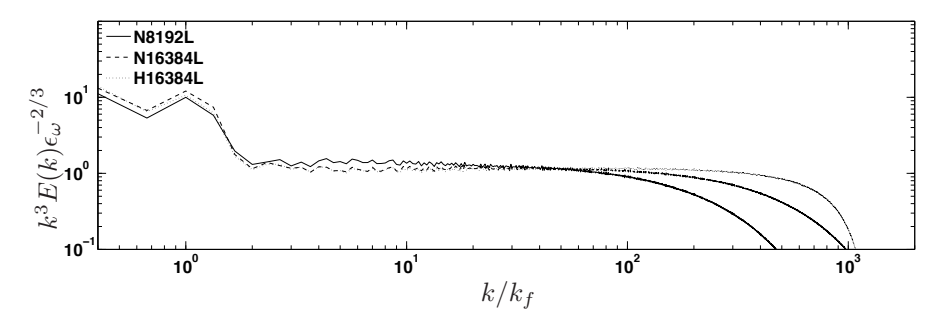


FIGURE 2.3. Compensated energy spectra, $k^3E(k)\epsilon_{\omega}^{-2/3}$, from a set of very high resolution simulations of forced two-dimensional turbulence.

of the forward enstrophy cascade. This cascade dominates the dynamics at several wave number decades, as shown in figure 2.3. However, the universality might fail with the constant \mathcal{C} , which has been found to vary in our simulations.

2.3. The energy cascade

A stationary inverse energy cascade range can only be obtained in the presence of a large scale drag, since energy would otherwise cascade indefinitely towards larger scales. In reality, there is a physical limit on how far the cascade can reach, namely the domain size. As energy reaches the smallest wave number, it will continuously pile up at this wave number, forming what is referred to as an Einstein-Bose condensate. Such a condensate can clearly bring the system away from the double cascade scenario by Kraichnan-Leith (e.g., Smith and Yakhot, 1994). In order to generate a double cascade with two wide inertial ranges, very high resolution simulations are required. Boffetta (2007) performed such simulations, showing a nearly perfect $k^{-5/3}$ inverse cascade range in presence of a linear Ekman drag, while obtaining an enstrophy inertial range a little steeper than k^{-3} , mainly for the highest resolution simulations. A linear drag is often introduced as a large-scale energy dissipation mechanism, found in real systems such as the atmosphere and in physical experiments. By investigating the fluxes of energy and enstrophy in physical space, Boffetta (2007) found that there is a very small correlation between the fluxes of these. This suggests that it should be possible to generate a single cascade of energy. This was also proposed by Tran and Bowman (2004). Therefore, it seems possible to force the fluid at scales near the small-scale dissipation range and obtain the classical $k^{-5/3}$ -spectra, despite dissipating nearly all enstrophy at the forcing scales. However, this suggestion has been cast in doubt. Starting with Borue (1994), it was found that the implementation of a large-scale hypodiffusion steepens the energy spectrum considerably to almost a k^{-3} -spectrum. The possible reason was found in the presence of vortices over all scales, whereas Boffetta et al. (2000) explained it in terms of a bottleneck effect as in three-dimensional turbulence (Falkovich, 1994). However, Smith and Yakhot (1994) found that the $k^{-5/3}$ -spectrum steepened to an exponent $\lesssim -2$ when resolving both of the cascades, as a consequence of vortex generation in the enstrophy cascade range. This result was later confirmed by Scott (2007), who provided estimates on when this steepening occurs by comparing the forcing wave number with the highest resolved wavenumber, based on high resolution simulations. A closer look at the results by Boffetta indicates that there is a small range located near the forcing scale in the inverse cascade, exhibiting a steeper slope than -5/3. To summarize, the issue seems rather involved, and there is no clear evidence for a universal and local energy inertial range, as also highlighted by Danilov and Gurarie (2001a, 2001b). As a response to these differing results, we have performed a set of high resolution simulations with and without a large scale linear drag of varying strength and with a variable forcing wave number. It has been found that the form of the energy spectrum is sensitive to the strength of the large scale drag. With the introduction of an infrared Reynolds number $Re_{\alpha} = k_f/k_{\alpha}$, where k_f is the forcing wave number and k_{α} is a frictional wave number, we demonstrate in paper 3 that the $k^{-5/3}$ energy spectrum steepens to k^{-2} or steeper at high Re_{α} .

2.4. Decaying turbulence

Decaying turbulence describes the evolution of a flow field in the absence of forcing and without any large scale dissipation, principally conserving energy at high Reynolds number. In that sense, decaying turbulence might be considered the purest case of two-dimensional turbulence. However, the initial conditions may differ considerably, although this should not cause any different results if the evolution is to be universal as predicted by Kraichnan-Batchelor-Leith. Therefore, it would seem natural that this case should be subject to less dispute. This is not the case. In fact, decaying 2D turbulence has been subject to renewed interest. As an initial flow field is released to decay freely, we could expect energy to cascade toward larger scales, where it is unaffected by smallscale viscosity, and so conserving energy, whereas the enstrophy would cascade toward smaller scales where it is dissipated. The question is how the energy spectrum evolves under these circumstances? According to Batchelor (1969), we could anticipate the survival of an enstrophy cascade, with an enstrophy spectrum scaling as $\Omega(k) \sim \epsilon_{\omega}^{2/3} k^{-1}$, where ϵ_{ω} is the enstrophy dissipation rate. This is the classical scenario. However, Dritschel et al. (2007) questioned this theoretical prediction. According to Dritschel et al. (2007), the enstrophy dissipation vanishes in the limit $\nu \to 0$ and this suggests that the enstrophy spectrum should instead scale as $\Omega(k) \sim \Omega k^{-1} (\ln Re)^{-1}$. However, we have performed a number of very high resolution simulations (as presented in paper 2) in which we find that Dritschel's argument that the inertial range should contain an increasing portion of the total enstrophy with time should be called into question. Thus, the relative enstrophy content has been found to increase at the lower wave number end, where a number of coherent vortices reside. Our simulations also show that the Batchelor-Kraichnan constant \mathcal{C} is of order unity, but varies, possibly as a consequence of extreme intermittency in the enstrophy dissipation, thus following the argument by Landau and Lifshitz (1987). In essence, we reproduced Batchelor's result, with a k^{-1} enstrophy spectrum in all our simulations, despite very different initial conditions, which are visible also at later times (see figure 2.4). Our results are illustrated in figure 2.5, which shows the compensated enstrophy spectra $k\Phi(k)\chi^{-2/3}$, where $\Phi(k)$ is the enstrophy spectrum and χ is the enstrophy dissipation rate, from three simulations with different initial conditions, taken at three instances in time. It is noteworthy that the steeper spectra obtained by earlier investigators (e.g., McWilliams, 1984 and Bartello and Warn, 1996), might be an artefact of a low Reynolds number, since the width of the enstrophy inertial range decreases slowly with time as the dissipation wave number $k_d \sim \epsilon_{\omega}^{1/6} \nu_{\omega}^{-1/2}$, and ϵ_{ω} decreases with time. We have also found that power law exponents of decay rates of quantities such as the enstrophy and hence enstrophy dissipation are dependent on the initial conditions. This has been shown also by van Bokhoven et al. (2007).

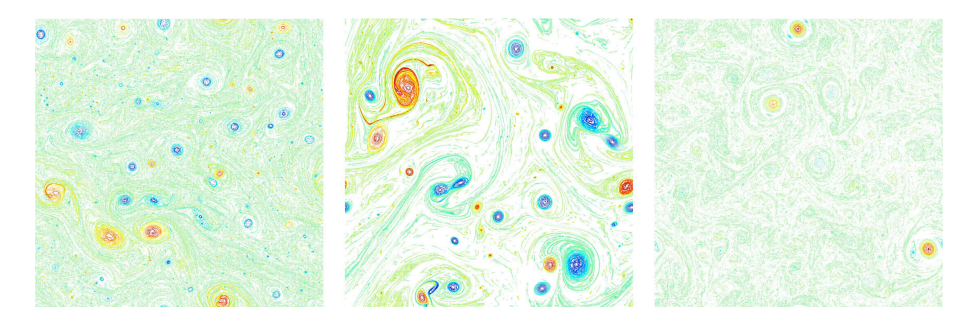


FIGURE 2.4. Snapshots of the "final" states from three simulations of decaying two-dimensional turbulence with various initial conditions. Red colour corresponds to positive vorticity and blue colour to negative vorticity.

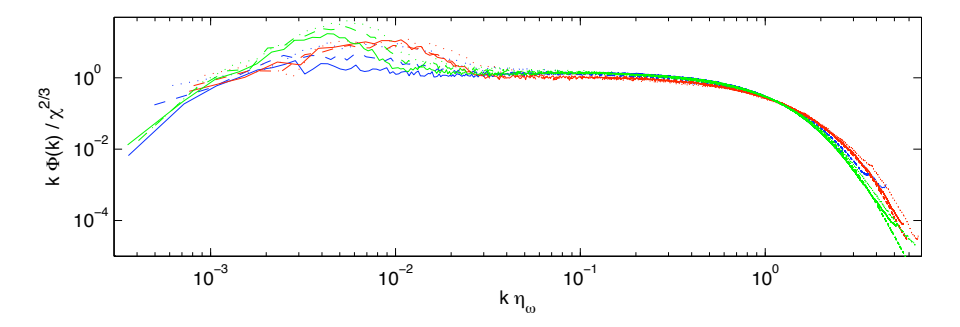


FIGURE 2.5. Compensated enstrophy spectra from three simulations (red, blue and green) of decaying two-dimensional turbulence, taken at three instances (solid, dashed and dotted) during each simulation. The abscissa is a nondimensional wavenumber, where $\eta_{\omega} = \nu^{1/2} \chi^{-1/6}$ is a characteristic scale of enstrophy dissipation.

2.5. Coherent structures

We have performed a number of simulations revealing the existence of strong and long-lived vortices which we refer to as coherent structures. They are easy to distinguish by the human eye as they stand out as ordered structures in a chaotic sea of filamentary vorticity debris (see figure 2.4). They are also belived to cause departures from universal scaling laws in two-dimensional turbulence. McWilliams (1984, 1990) found early evidence of stuctures containing a substantial fraction of vorticity of two-dimensional flows, with lifetimes far exceeding the characteristic time for nonlinear interactions. He found that vortices spontaneously develop if the forcing and friction is relatively weak and the Reynolds number sufficiently high. They are approximately axisymmetric and

are stable to perturbations from the quiescent surroundings but not to encounters by other strong vortices, which could result in like-sign vortex mergers. McWilliams (1990) noted that the lock-up of vorticity inside coherent vortices effectively reduces cascade rates of both enstrophy and energy. By introducing a vortex-census algorithm, he enabled detailed studies of their properties and found a general trend of the "survival of the fittest". Dritschel (1995) contributed with a detailed study of vortex interactions and showed that these are relatively short inelastic interactions resulting in two or three new coherent vortices, thus questioning the picture of the inverse energy cascade as a series of merging events resulting in ever-growing vortices, as suggested by, e.g., Borue (1994), in forced two-dimensional turbulence. In decaying turbulence, it is more evident that large-scale structures form as a result of vortex mergers, finally resulting in two opposite-sign vortices (Tabeling, 2002). An interesting question is whether any universal theory can account for coherent vortices. Carnevale et al. (1991) suggested such a theory for vortex circulation, radius, mean enstrophy and kurtosis, but there are ample examples of deviations from such a governing theory (Tabeling, 2002).

2.6. β -plane turbulence

To accommodate for a background rotation, a β -plane approximation has been introduced to the 2D Navier-Stokes equation;

$$\frac{\partial \omega}{\partial t} + (\boldsymbol{u} \cdot \nabla)\omega = -\nu \nabla^2 \omega - \beta v. \tag{2.16}$$

The β -term arises from the following argument. We consider a rotating sphere such as illustrated in figure 2.6. and note that the Coriolis force $2\Omega \times \mathbf{u}$ can be rewritten by defining

$$f \equiv 2\Omega \sin \phi e_z, \tag{2.17}$$

where \mathbf{e}_z is the normal unit vector to a locally Cartesian tangent plane on the sphere. For small variations in the meridional direction

$$f = 2\Omega \sin \phi \simeq 2\Omega \sin \phi_0 + 2\Omega(\phi - \phi_0) \cos \phi_0, \tag{2.18}$$

and we approximate the Coriolis parameter to vary linearly on the tangent plane as

$$f = f_0 + \beta y, \tag{2.19}$$

where

$$f_0 = 2\Omega \sin \phi_0. \tag{2.20}$$

Thus

$$\beta = \frac{df}{dy} = \frac{2\Omega\cos\phi_0}{R_{\oplus}},\tag{2.21}$$

where R_{\oplus} is the radius of the Earth, and equation (2.16) approximately describes the motions on a rotating sphere, provided that the flow is spatially limited so that the geometric effects of sphericity are negligible, and is known as the β -plane approximation. It allows for the use of a local Cartesian representation of the Navier-Stokes equation, while still capturing the important

dynamical effects stemming from sphericity and is dynamically equivalent to a differentially rotating system.

We thus see the existence of an additional term βv on the right hand side. We may now ask what dynamical consequences the inclusion of this term might have. Rhines (1975) investigated this matter and showed that turbulent energy is dispersed into waves at scales larger than approximately

$$k_{\beta} = \sqrt{\frac{\beta}{2\sqrt{\overline{E}}}},\tag{2.22}$$

where \overline{E} is the r.m.s. energy of the flow. This scale is approximate and there exists a number of definitions of this arrest scale, which do not differ too much. Thus, the inverse energy cascade continues up to a scale k_{β} , from which no upscale energy cascade is possible. Instead, the transition to wave propagation (Rossby waves) is overtaken by a flow characterized by steady alternating zonal jets. This picture is helpful in explaining the characteristic size of eddies in the Earth's atmosphere, and the prevalence of zonal flows. The waves are referred to as Rossby waves, and its dispersion relation can be obtained by linearizing (2.16) upon a basic state with a perturbation. Rossby waves are an important ingredient in atmospheric dynamics, with large effects on both daily weather and regional climate. Many numerical experiments over the years have to a large degree verified Rhines' prediction. Maltrud and Vallis (1991) found that the β -effect tend to destroy coherent vortices at large scales but that the resulting anisotropy at scales larger than k_{β} does not influence the inertial range characteristics at smaller scales. Later studies have concerned the statistical characteristics of the resulting zonal jets (e.g., Vallis and Maltrud, 1993; Manfroi and Young, 1998; Danilov and Gurarie, 2004). It is noteworthy that attempts have been made to explain the atmospheric flow structure on Jupiter, with its zonal jets and superstationary vortices, in terms of two-dimensional or quasigeostrophic turbulence with a β -effect (e.g., Kukharkin and Orszag, 1996; Smith, 2004). An example of a simulation with a β -effect is shown in figure 2.7 (left), where the anisotropy at large scales is clearly visible. Figure 2.7 (right) also shows a satellite image of Jupiter, with the characteristic zonal flow and the famous red spot visible as a coherent vortex in the southern hemisphere.

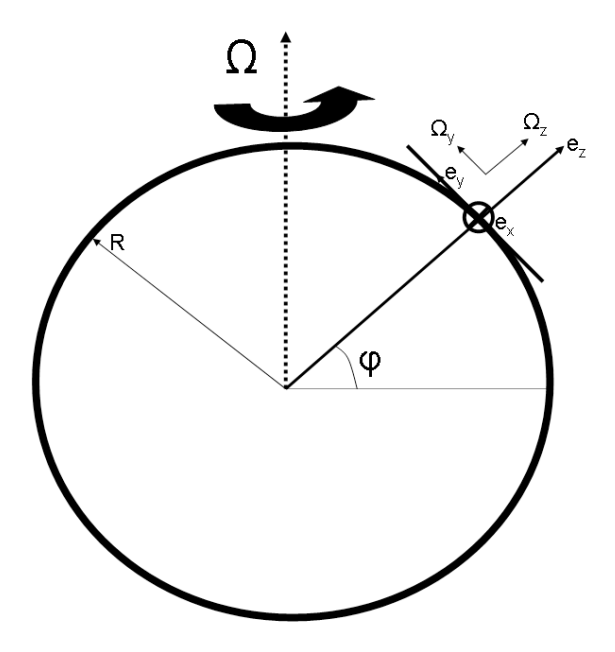


FIGURE 2.6. Tangent plane approximation to the quasispherical Earth. The rotation vector components in the plane are shown as well as the direction of the unit vectors.

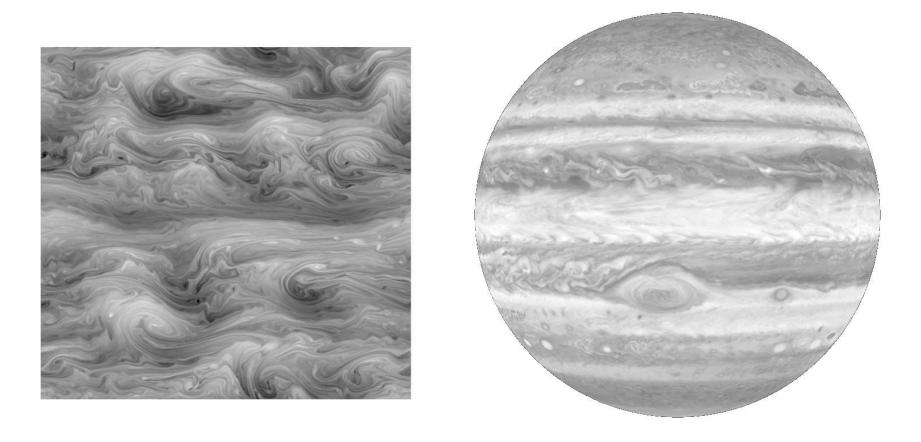


FIGURE 2.7. Left: vorticity snapshot from a simulation with moderate β . Right: satellite image of Jupiter's atmosphere (from NOAA).

CHAPTER 3

Quasigeostrophic turbulence

So far, we have considered two-dimensional turbulence. In many natural systems, such as the atmosphere, there is a vertical stratification. Horizontal variations of the density introduces potential energy into the system, which can be released by the excitation of baroclinic motions. These motions are manifested in the atmosphere by the development of cyclones and anticyclones in the midlatitudes, largely responsible for the day-to-day weather we experience. These systems are generally fully developed at scales $\sim 1000~\rm km$ and can in part be studied within the framework of QG turbulence. The dynamics is described by the QG potential vorticity equation, which is given by

$$\frac{\partial q}{\partial t} + (\mathbf{u_h} \cdot \nabla_h) q + \beta v = (-1)^{n+1} \nu_q \nabla^{2n} q + f + (-1)^{p+1} \nu_u \nabla^{-2p} q, \qquad (3.1)$$

where

$$q = \nabla^2 \psi \tag{3.2}$$

is the QG potential vorticity, Δ is the three-dimensional Laplace operator in scaled coordinates, ψ is the stream function, $\mathbf{u_h} = u\mathbf{e_x} + v\mathbf{e_v} = -\partial_y \psi \mathbf{e_x} + \partial_x \psi \mathbf{e_v}$ is the horizontal velocity and ∇_h is the horizontal gradient operator, ν_q is the hyperviscosity coefficient and ν_u is an optional hypofriction (p > 0) or Ekman drag (p = 0) coefficient. For a complete derivation of this equation, see appendix A. The most important property of this equation is the inviscid conservation of potential vorticity. Note also that the quasigeostrophic motion is in the horizontal plane but that these motions generally vary in the vertical. This turbulent regime was theoretized by Charney (1971). By scaling the vertical coordinate by N/f, he argued that the flow field should obey a special type of isotropy, which has been given the name Charney isotropy, after Charney (1971). Charney isotropy means that the energy spectrum, in the scaled variables, is invariant in the different directions (e.g., horizontal and vertical). Charney also predicted approximate equipartition between kinetic and potential energy in the three-dimensional energy spectra. The prediction of Charney isotropy has been supported by numerical experiments such as Hua and Haidvogel (1986) and McWilliams (1989).

Just as in two-dimensional turbulence, there is rich dynamics in the flow (see figure 3.1), with the development of coherent structures under favourable conditions. The presence of a vertical dimension introduces new features of these vortices, which can be barotropic or baroclinic to various degrees, and

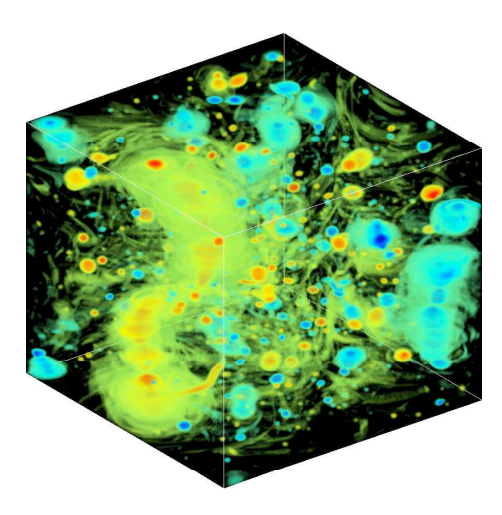


FIGURE 3.1. Potential vorticity snapshot from a freely decaying quasigeostrophic simulation. Red (blue) colour corresponds to positive (negative) potential vorticity.

for a thorough review of their statistical properties, it is recommended to consult, e.g., McWilliams (1990), McWilliams et al. (1999), von Hardenberg et al. (2000) and Reinaud et al. (2003). In paper 4, we present results on a series of high resolution simulations that essentially confirm Charney's predictions under a wide range of conditions and the similarities with 2D turbulence. Furthermore, it is shown that the prediction might even be stronger than Charney anticipated, since the general picture holds qualitatively also in presence of a planetary vorticity gradient. It is also suggested in appendix A, that there is the potential of extending the quasigeostrophic regime to scales approximately equal to the deformation radius.

CHAPTER 4

Numerical method and the codes

Two pseudospectral codes, PNSE2D and QGE3D have been developed to solve the two-dimensional Navier-Stokes and Charney QG potential vorticity equation, respectively. The codes have been written in Fortran90. Pseudospectral means that the time-stepping is performed in spectral space whereas the nonlinear products are calculated in real space. Fourier transforms are calculated with the aid of an efficient FFT-package called FFTW. Time-stepping is performed with a Runge-Kutta fourth order scheme and the time step is determined using a CFLcondition. Viscosity, being it small scale Navier-Stokes viscosity, hyperviscosity or large scale hypodiffusion or linear Ekman drag, is calculated with the use of an integrating factor technique. The codes are essentially free from aliasing errors by the use of an 8/9-dealiasing technique, which allows for a wider range of Fourier modes to be captured compared to the traditional 2/3-dealiasing. For a more thourough review of the details of the codes, see paper 5, which also discusses some statistical measures and parallelisation approaches. It should be noted that the codes have been customized to run on massively parallel super computers, to allow for very high resolution simulations. A survey of the speedup of the codes is also presented in paper 5.

CHAPTER 5

Summary of the papers

Paper 1

The enstrophy cascade in forced two-dimensional turbulence. This paper investigates the enstrophy cascade in forced two-dimensional turbulence by performing a set of high resolution simulations with different forcing wave numbers. One of the simulations is larger than any other simulation presented in the literature so far. In the absence of a large-scale drag, we obtain Kraichnan's original prediction (1967) of a clean k^{-3} energy spectrum in the enstrophy inertial range. However, it is found that the Kraichnan constant varies slightly between the simulations and is decreasing very slowly with time. When forcing is applied at relatively large wave number, we obtain coherent vortices at scales larger than the forcing scale, and intermittency measures become very large at all scales. However, when forcing is applied at small wave number, intermittency statistics are close to Gaussian. The main conclusion is that the enstrophy cascade is a robust feature of two-dimensional turbulence.

Paper 2

Testing Batchelor's similarity hypothesis for decaying two-dimensional turbulence. This paper studies the enstrophy cascade in decaying two-dimensional turbulence to test Batchelor's hypothesis of an equilibrium range. By performing three simulations with very different initial conditions, Batchelor's hypothesis is corroborated. As in paper 1, it is found that the Batchelor-Kraichnan constant varies. It is ~ 1.4 in two of the simulations and ~ 1.1 in one. It is hypothesized that a higher degree of intermittency of dissipation causes the constant to be lower in one of the simulations.

Paper 3

Infrared Reynold's number dependency of the two-dimensional inverse energy cascade. In this paper, the inverse energy cascade is subject to high resolution numerical experiments. A surprising result is found, showing that the $k^{-5/3}$ -scaling in the inertial energy range is likely to be a low frictional Reynolds number effect, in presence of a large-scale linear friction. When the inertial energy range is wide enough, the linear friction is too weak at the forcing scales to prevent the formation of coherent vortices. These act to steepen the energy

spectrum from $k^{-5/3}$ to k^{-2} or steeper. The linear friction is shown to impose a larger effect than the ultraviolet dissipation.

Paper 4

Charney isotropy and equipartition in quasigeostrophic turbulence. This paper is devoted to studies of quasigeostrophic turbulence, as theoretized by Charney (1971). We verify Charney's predictions of isotropy and equipartition by performing high resolution three-dimensional simulations. It is also demonstrated that Charney's predictions also holds in the presence of a β -effect and in freely decaying quasigeostrophic turbulence. The analogy with two-dimensional turbulence is investigated and confirmed.

Paper 5

Simulations of two-dimensional and quasigeostrophic turbulence: Technical Report. Paper 5 is a technical report that describes the two codes in greater detail. The code structures are explored and underlying assumptions, statistical measures and code performance are presented for each code, respectively. The codes are found to scale well in massively parallel systems and they allow for cutting edge numerical experiments.

CHAPTER 6

Outlook

It has become clear that Kraichnan's and Batchelor's predictions on the form of the energy spectrum in the enstrophy inertial range are robust at high Reynolds number. Earlier investigations found steeper energy spectrum and it was believed to be an effect of intermittency. Our results suggest that intermittency only affects the Batchelor-Kraichnan constant and not the k^{-3} -scaling. We now believe we are in a position to interpret this fact as a consequence of intermittency in the enstrophy dissipation. This was originally addressed by Landau and Lifshitz (1987), who concluded that the spatial variance of the dissipation is nonuniversal and could thus not result in a universal averaging of the dissipation. Kraichnan (1974) elaborated on this argument, and concluded that this is a result of spatial averaging over the domain scale, which contains patches of enhanced dissipation larger than the inertial scales, which we aim to describe. Thus, when determining the dissipation rates, it should be taken as an ensemble average of smaller subdomains making up the whole flow field, since the average $\epsilon_{\omega}^{-} = \langle \epsilon_{\omega}^{2/3} \rangle$ is different from $\epsilon_{\omega}^{-2/3}$. In paper 2, we suggest that the small variation observed in the constant may be explained as a consequence of intermittency. In a revision of paper 1, this hypothesis will be quantitatively investigated. Perhaps of greater physical interest, is to extend the quasigeostrophic framework to the primitive equations, which are a set of nonlinear equations used in atmospheric and oceanic modeling (Vallis, 2006). The equation set contains the momentum equations in the horizontal, the hydrostatic approximation in the vertical and is completed by the thermodynamic and continuity equations. The use of the primitive equations allows for variations of the Rossby deformation radius by varying the stratification, which is fixed in the framework of Charney quasigeostropy. By doing this, we aim to explore the dynamic origins of the atmospheric energy spectrum and determine the origin of the high wave number $k^{-5/3}$ -range.

Acknowledgements

First of all I would like to thank my supervisor Dr. Erik Lindborg for all his help and patience during the past three years. It has been a long and enjoyable journey, with many good laughs but also a scientific adventure with many unexpected outcomes. I would also like to thank my co-advisor Geert Brethouwer for his help with getting me started in the implementation of the codes. A great thank you also to Philipp Schlatter, who has given me good advices in order to increase the performance of the codes. The working environment has been very pleasant thanks to both a good atmosphere but also thanks to the students in Dan Henningson's group and Andreas Carlson, my current office colleagues Amin Rasam and Enrico Deusebio, but also former roomies Niklas Mellgren and Seif Dalilsafaei. The list would not be complete without a thank you to my colleagues at the Swedish Television, in particular Pär Holmgren and Helen Johansson, who have enabled me to stay in touch with the real world of meteorology and climate. Something which also Jenny Brandefelt have made possible. Thanks also to Johan Liakka at Stockholm University, whom I have shared thoughts and ideas with every now and then. I would also like to gratefully acknowledge the Linné FLOW centre, financed by the Swedish Research Council (Vetenskapsrådet), for funding of the project. SNIC (Swedish National Infrastructure for Computing) is acknowledged for computer time at the Centre for Parallel Computers (PDC) at the Royal Institute of Technology in Stockholm and the National Supercomputer Centre (NSC) in Linköping, with a generous grant by the Knut and Alice Wallenberg (KAW) foundation. Last, but not the least, I would like to thank Liisa for her love, patience and encouragement.

APPENDIX A

Derivation of the QG potential vorticity equation

A.1. Introduction

This appendix gives an introduction to the dynamics of the midlatitude troposphere and more specifically the quasigeostrophic equations. These are a specific set of equations that describes the synoptic scale motions in a bounded domain on a rotating sphere such as the Earth. The aim is to derive a relevant formulation of the quasigeostrophic potential vorticity equation. The starting point will be the 3D Navier-Stokes equation on a rotating sphere, from which we will systematically exploit the involved terms on our way to quasigeostrophy following Pedlosky (1987).

A.2. Scaling the 3D Navier-Stokes equation

We consider motions on a rotating sphere of radius r_0 , ignoring the slight departure from sphericity of the Earth. We assume that the vertical scale of motion is small enough so that the gravitational acceleration can be considered constant through the depth of the fluid. In addition, we assume that the scales are large enough so that viscous effects can be ignored. Since we can anticipate that the geostrophic approximation must fail near the equator, the theory must apply to a spatial extent that is less than global. Hence, the restriction is that $O\left(\frac{L}{r_0}\right) < 1$. The spherical coordinate system is defined in such a way that the radius \mathbf{r} defines the surface-normal direction, whereas θ is the latitude and ϕ is the longitude. Neglecting viscous effects, friction and forcing, the momentum and mass continuity equations are given by

$$\frac{D\boldsymbol{u}}{Dt} + 2\boldsymbol{\Omega} \times \boldsymbol{u} = -\frac{1}{\rho} \nabla p + \boldsymbol{g}, \tag{A.1}$$

$$\frac{D\rho}{Dt} + \rho \nabla \cdot \boldsymbol{u} = 0, \tag{A.2}$$

$$\frac{D}{Dt} \equiv \frac{\partial}{\partial t} + \boldsymbol{u} \cdot \nabla. \tag{A.3}$$

In spherical coordinates, the mass continuity equation can be expressed as

$$\frac{D\rho}{Dt} + \rho \left[\frac{1}{r^2} \frac{\partial (r^2 w)}{\partial r} + \frac{1}{r \cos \theta} \frac{\partial (v \cos \theta)}{\partial \theta} + \frac{1}{r \cos \theta} \frac{\partial u}{\partial \phi} \right] = 0, \tag{A.4}$$

$$\frac{D}{Dt} = \frac{\partial}{\partial t} + \frac{u}{r\cos\theta} \frac{\partial}{\partial \phi} + \frac{v}{r} \frac{\partial}{\partial \theta} + w \frac{\partial}{\partial r}.$$
 (A.5)

Now let

$$\mathbf{u} = u\hat{\boldsymbol{\phi}} + v\hat{\boldsymbol{\theta}} + w\hat{\boldsymbol{r}},\tag{A.6}$$

$$u \equiv r \cos \theta \frac{D\phi}{Dt},\tag{A.7}$$

$$v \equiv r \frac{D\theta}{Dt},\tag{A.8}$$

$$w \equiv \frac{Dr}{Dt}.\tag{A.9}$$

Hence,

$$\frac{D\boldsymbol{u}}{Dt} = \hat{\boldsymbol{\phi}} \frac{D\boldsymbol{u}}{Dt} + \hat{\boldsymbol{\theta}} \frac{D\boldsymbol{v}}{Dt} + \hat{\boldsymbol{r}} \frac{D\boldsymbol{w}}{Dt} + u \frac{D\hat{\boldsymbol{\phi}}}{Dt} + v \frac{D\hat{\boldsymbol{\theta}}}{Dt} + w \frac{D\hat{\boldsymbol{r}}}{Dt}. \tag{A.10}$$

Similarity consideration shows that

$$\lim_{\delta x \to 0} \frac{|\delta \hat{\phi}|}{\delta x} = \frac{1}{r \cos \theta},\tag{A.11}$$

$$\frac{\delta \hat{\boldsymbol{\phi}}}{\delta x} = \frac{1}{r \cos \theta} \left(\hat{\boldsymbol{\theta}} \sin \theta - \hat{\boldsymbol{r}} \cos \theta \right), \tag{A.12}$$

$$\frac{D\hat{\phi}}{Dt} = \frac{u}{r\cos\theta} \left(\hat{\boldsymbol{\theta}} \sin\theta - \hat{\boldsymbol{r}} \cos\theta \right), \tag{A.13}$$

and equivalently for the $\hat{\theta}$ and \hat{r} unit vectors it can be shown that

$$\frac{D\hat{\boldsymbol{\theta}}}{Dt} = -\frac{u\tan\theta}{r}\hat{\boldsymbol{\phi}} - \frac{v}{r}\hat{\boldsymbol{r}},$$

$$\frac{D\hat{\boldsymbol{r}}}{Dt} = \frac{u}{r}\hat{\boldsymbol{\phi}} + \frac{v}{r}\hat{\boldsymbol{\theta}}.$$
(A.14)

$$\frac{D\hat{r}}{Dt} = \frac{u}{r}\hat{\phi} + \frac{v}{r}\hat{\theta}.$$
 (A.15)

Thus, the acceleration following the relative motion in spherical coordinates is

$$\frac{D\boldsymbol{u}}{Dt} = \hat{\boldsymbol{\phi}} \left(\frac{D\boldsymbol{u}}{Dt} - \frac{u\boldsymbol{v}\tan\theta}{r} + \frac{u\boldsymbol{w}}{r} \right) + \hat{\boldsymbol{\theta}} \left(\frac{D\boldsymbol{v}}{Dt} + \frac{u^2\tan\theta}{r} + \frac{v\boldsymbol{w}}{r} \right) + \hat{\boldsymbol{r}} \left(\frac{D\boldsymbol{w}}{Dt} - \frac{u^2 + v^2}{r} \right). \tag{A.16}$$

Expansion of the Coriolis term in spherical coordinates is now demonstrated below;

$$2\mathbf{\Omega} \times \mathbf{u} = 2\Omega \begin{vmatrix} \hat{\boldsymbol{\phi}} & \hat{\boldsymbol{\theta}} & \hat{\boldsymbol{r}} \\ 0 & \cos \theta & \sin \theta \\ u & v & w \end{vmatrix} = 2\Omega \left[(w\cos \theta - v\sin \theta) \,\hat{\boldsymbol{\phi}} + u\sin \theta \hat{\boldsymbol{\theta}} - u\cos \theta \hat{\boldsymbol{r}} \right].$$
(A.17)

The pressure gradient and gravity are trivially expressed and can easily be identified in the component form of (A.1), as shown below:

$$\frac{Du}{Dt} + \frac{uw}{r} - \frac{uv}{r}\tan\theta + 2\Omega w\cos\theta - 2\Omega v\sin\theta = -\frac{1}{\rho r\cos\theta}\frac{\partial p}{\partial \phi}, \quad (A.18)$$

$$\frac{Dv}{Dt} + \frac{vw}{r} + \frac{u^2}{r}\tan\theta + 2\Omega u\sin\theta = -\frac{1}{\rho r}\frac{\partial p}{\partial \theta},$$
 (A.19)

$$\frac{Dw}{Dt} - \frac{u^2 + v^2}{r} - 2\Omega u \cos \theta = -\frac{1}{\rho} \frac{\partial p}{\partial r} - g.$$
 (A.20)

The momentum and mass continuity equation need to be complemented by the thermodynamic equation;

$$\frac{D\theta}{Dt} = \frac{\theta}{c_p T} \left(\frac{k}{\rho} \nabla^2 T + Q \right), \tag{A.21}$$

where k is the thermal conductivity, T the temperature, Q the rate of heat addition per unit mass by internal heat sources and θ is the potential temperature, defined as

$$\theta = T \left(\frac{p_0}{p}\right)^{\frac{R}{c_p}}. (A.22)$$

Note that p, ρ and T are related by the ideal gas law;

$$p = \rho RT. \tag{A.23}$$

Now, we consider motions, whose horizontal spatial scale of variation is given by the length scale L and velocity scale U. Furthermore, we restrict ourselves to the mid-latitude region centred at around some latitude θ_0 . In addition, we restrict ourselves to Cartesian coordinates by replacing the spherical coordinates as follows

$$\begin{cases} x = \phi r_0 \cos \theta_0, \\ y = r_0(\theta - \theta_0), \end{cases}$$
 (A.24)

and hence

$$\begin{cases} \frac{\partial}{\partial \phi} = r_0 \cos \theta_0 \frac{\partial}{\partial x}, \\ \frac{\partial}{\partial \theta} = r_0 \frac{\partial}{\partial y}. \end{cases}$$
(A.25)

In addition, the following substitutions are introduced

$$\begin{cases}
z = r - r_0 = Dz', \\
x = Lx', \\
y = Ly', \\
t = \frac{L}{U}t', \\
u = Uu', \\
v = Uv', \\
w = \frac{D}{L}Uw'.
\end{cases}$$
(A.26)

Note that the time scales advectively. We now turn to the hydrostatic approximation;

$$\frac{\partial p_s}{\partial z} = -\rho_s(z)g,\tag{A.27}$$

where the subscript s denotes a standard basic state upon which perturbations occur such that

$$\begin{cases}
p = p_s(z) + \tilde{p}(x, y, z, t), \\
\rho = \rho_s(z) + \tilde{\rho}(x, y, z, t).
\end{cases}$$
(A.28)

We need to scale the pressure and density pertubations in some sense. It can be conjectured that for the motions of interest, the horizontal pressure gradient will be of the same order of magnitude as the Coriolis acceleration, i.e., $\mathcal{O}(\rho_s 2\Omega u \sin \theta_0) \sim \mathcal{O}\left(\frac{\tilde{p}}{L}\right) \rightarrow \tilde{p} \sim \mathcal{O}(\rho_s U f_0 L)$, where

$$f_0 = 2\Omega \sin \theta_0, \tag{A.29}$$

is the Coriolis parameter at θ_0 . Hence,

$$p = p_s(z) + \rho_s(z)Uf_0Lp'. \tag{A.30}$$

In a similar manner, we may anticipate that the buoyancy force due to $\tilde{\rho}$ will be of the same order of magnitude as the vertical pressure gradient by recalling the hydrostatic approximation, upon which $\frac{\partial \tilde{p}}{\partial z} = \mathcal{O}\left(\frac{\tilde{p}}{D}\right) = \mathcal{O}\left(\frac{\rho_s U f_0 L}{D}\right) \sim$

$$\mathcal{O}(\tilde{\rho}g) \to \mathcal{O}(\tilde{\rho}) = \mathcal{O}\left(\rho_s U \frac{f_0 L}{gD}\right)$$
. Hence, we may write

$$\rho = \rho_s(z) \left[1 + Ro \ F \rho' \right], \tag{A.31}$$

where

$$\begin{cases}
Ro \equiv \frac{U}{f_0 L} \equiv \epsilon, \\
F = \frac{f_0^2 L^2}{gD}.
\end{cases}$$
(A.32)

Here, $Ro = \epsilon$ is the Rossby number. We are now at the point where the momentum equation components can be non-dimensionalized following the substitutions addressed so far. Thus, applying (A.26), (A.27), (A.30) and (A.31) to the component momentum equations and dividing through by Uf_0 , we obtain

$$\epsilon \left[\frac{Du'}{Dt'} + \frac{L}{r_*} \left(\delta u' w' - u' v' \tan \theta \right) \right] - v' \frac{\sin \theta}{\sin \theta_0} + \delta w' \frac{\cos \theta}{\sin \theta_0} =$$

$$= -\frac{r_0}{r_*} \frac{\cos \theta_0}{\cos \theta} \frac{1}{1 + \epsilon F \rho'} \frac{\partial p'}{\partial x'}, \quad (A.33)$$

$$\epsilon \left[\frac{Dv'}{Dt'} + \frac{L}{r_*} \left(\delta v'w' + u'^2 \tan \theta \right) \right] + u' \frac{\sin \theta}{\sin \theta_0} = -\frac{r_0}{r_*} \frac{1}{1 + \epsilon F \rho'} \frac{\partial p'}{\partial y'}, \quad (A.34)$$

$$D(1 + \epsilon F \rho') \left[U^2 \left(\frac{D}{L^2} \frac{Dw'}{Dt'} - \frac{u'^2 + v'^2}{r_*} \right) - 2\Omega U u' \cos \theta \right] =$$

$$= -\frac{1}{\rho_s} \frac{\partial}{\partial z'} \left[p_s + U f_0 L \rho_s \rho' \right] - D(1 + \epsilon F \rho') g_*, \quad (A.35)$$

where the subscript * denotes dimensional quantities and

$$\delta \equiv \frac{D}{L}.\tag{A.36}$$

The vertical component (A.35) can be further simplified by expansion of the right hand side to yield, after division by Uf_0L ;

$$(1 + \epsilon F \rho') \left[\epsilon \delta^2 \frac{Dw'}{Dt'} - \frac{\epsilon \delta L}{r_*} (u'^2 + v'^2) - \delta u' \frac{\cos \theta}{\sin \theta_0} \right] = -\frac{1}{\rho_s} \frac{\partial}{\partial z'} (\rho_s p') - \rho'.$$
(A.37)

The nondimenzionalized total derivative takes the following form

$$\frac{D}{Dt'} = \frac{\partial}{\partial t'} + u' \frac{r_0}{r_*} \frac{\cos \theta_0}{\cos \theta} \frac{\partial}{\partial x'} + v' \frac{r_0}{r_*} \frac{\partial}{\partial y'} + w' \frac{\partial}{\partial z'}.$$
 (A.38)

Note that

$$\frac{r_*}{r_0} = 1 + \delta\left(\frac{L}{r_0}\right)z'. \tag{A.39}$$

Expanding the mass continuity equation (A.4) and applying the substitutions result in the nondimensional version

$$\epsilon F \frac{D\rho'}{Dt'} + (1 + \epsilon F\rho') \left[\frac{w'}{\rho_s} \frac{\partial \rho_s}{\partial z'} + \frac{\partial w'}{\partial z'} + 2 \frac{D}{r_*} w' + \frac{r_0}{r_*} \frac{\partial v'}{\partial y'} + - \frac{L}{r_*} v' \tan \theta + \frac{r_0}{r_*} \frac{\cos \theta_0}{\cos \theta} \frac{\partial u'}{\partial x'} \right] = 0. \quad (A.40)$$

In the following, the superscripts' denoting the nondimensional variables will be dropped and the subscript * will denote dimensional remnants in the equations. It is important to note that no restrictive approximations have been applied so far. The equations have just been scaled so that their relative magnitude can be estimated by the nondimensional parameters multiplying the individual terms. Before investigating any specific parameter settings, we expand the trigonometric terms around the θ_0 -latitude in Taylor expansions, i.e.,

$$\sin \theta = \sin \theta_0 + \frac{d(\sin \theta)}{d\theta}|_{\theta = \theta_0} (\theta - \theta_0) + \frac{d^2(\sin \theta)}{d\theta^2}|_{\theta = \theta_0} \frac{(\theta - \theta_0)^2}{2!} + \dots \quad (A.41)$$

With the use of (A.24) and (A.26) we thus obtain

$$\begin{cases} \sin \theta = \sin \theta_0 + \frac{L}{r_0} y \cos \theta_0 - \frac{1}{2} \left(\frac{L}{r_0}\right)^2 y^2 \sin \theta_0 + \dots, \\ \cos \theta = \cos \theta_0 - \frac{L}{r_0} y \sin \theta_0 - \frac{1}{2} \left(\frac{L}{r_0}\right)^2 y^2 \cos \theta_0 + \dots, \\ \tan \theta = \tan \theta_0 + \frac{L}{r_0} y \frac{1}{\cos^2 \theta_0} + \left(\frac{L}{r_0}\right)^2 y^2 \frac{\tan \theta_0}{\cos^2 \theta_0} + \dots, \end{cases}$$
(A.42)

Last, but not the least, we now define the β -parameter as

$$\beta_0 = \frac{d}{dy} \left(2\Omega \sin \theta \right) |_{\theta = \theta_0} = \frac{1}{r_0} \frac{d}{d\theta} \left(2\Omega \sin \theta \right) |_{\theta = \theta_0} = \frac{2\Omega}{r_0} \cos \theta_0 \tag{A.43}$$

It can be noted here that $\frac{\beta_0 L}{f_0} = \dots = \frac{L}{r_0} \cot \theta_0 \sim \mathcal{O}\left(\frac{L}{r_0}\right)$ and hence $\frac{\beta_0 L}{f_0} = \frac{\beta_0 L^2}{U} \sim \mathcal{O}\left(\frac{L}{\epsilon r_0}\right)$ so that the magnitude of the relative vorticity- to the planetary

vorticity gradient is measured by

$$\frac{1}{\beta} = \frac{U}{\beta_0 L^2} \sim \mathcal{O}\left(\epsilon \frac{r_0}{L}\right),\tag{A.44}$$

which is evidentally determined by the relative size of the Rossby number and the inverse ratio between the horizontal length scale and approximately the Earth's radius for tropospheric considerations.

A.3. The geostrophic approximation

So far, no specific scale of motion has been chosen. By noting that in the midlatitude atmosphere,

$$\begin{cases}
U \sim \mathcal{O}(10 \ ms^{-1}), \\
L \sim \mathcal{O}(1000 \ km), \\
D \sim \mathcal{O}(10 \ km), \\
f_0 \sim \mathcal{O}(10^{-4} \ s^{-1}),
\end{cases}$$
(A.45)

we first choose to study the case $\epsilon \sim \mathcal{O}\left(\frac{L}{r_0} << 1\right)$, i.e., motions that are less than global. Under these circumstances, $\frac{U}{\beta_0 L^2} \sim \mathcal{O}\left(\frac{10}{10^{-11}(10^6)^2}\right) \sim \mathcal{O}(1)$. Thus, the planetary vorticity gradient is expected to play an active role in the atmospheric dynamics at this horizontal length scale. Making use of (A.45), we can summarize the key parameters as

$$\begin{cases} \epsilon \sim \mathcal{O}(10^{-1}), \\ \beta \sim \mathcal{O}(1), \\ F = \frac{f_0^2 L^2}{gD} \sim \mathcal{O}(10^{-1}) \sim O(\epsilon), \\ \frac{L}{r_0} \sim \mathcal{O}(\epsilon), \\ \delta = \frac{D}{L} \sim \mathcal{O}(10^{-2}) \sim \mathcal{O}(\epsilon^2), \\ \frac{r_*}{r_0} - 1 \sim \mathcal{O}\left(\delta \frac{L}{r_0}\right) \sim \mathcal{O}(\epsilon^3), \end{cases}$$
(A.46)

The limit $\epsilon \to 0$, $\frac{\epsilon r_0}{L} \sim \mathcal{O}(1)$, is a special case that examines geostrophic dynamics when the planetary vorticity gradient contributes equally to the relative vorticity gradient. We now express all the dynamic variables, i.e., u, v, w, p, ρ , in series of the key parameter ϵ such that

$$u(x, y, z, t) = u_0(x, y, z, t) + \epsilon u_1(x, y, z, t) + \epsilon^2 u_2(x, y, z, t) + \dots etc. \quad (A.47)$$

Applying (A.42), (A.46) and the first two terms of (A.47) for the dynamic variables to (A.33), (A.34) and (A.37), we obtain

$$\epsilon \left[\frac{D(u_0 + \epsilon u_1)}{Dt} + \frac{L}{r_*} \left(\epsilon^2 (u_0 + \epsilon u_1)(w_0 + \epsilon w_1) + \frac{L}{r_0} \cos^{-2} \theta_0 \right) \right] + \\
- (u_0 + \epsilon u_1)(v_0 + \epsilon v_1) \left(\tan \theta_0 + \frac{Ly}{r_0} \cos^{-2} \theta_0 \right) \right] + \\
- (v_0 + \epsilon v_1) \frac{\left(\sin \theta_0 + \frac{Ly}{r_0} \cos \theta_0 \right)}{\sin \theta_0} + \epsilon (w_0 + \epsilon w_1) \frac{\left(\cos \theta_0 - \frac{Ly}{r_0} \sin \theta_0 \right)}{\sin \theta_0} = \\
= -\frac{r_0}{r_*} \frac{\cos \theta_0}{\left(\cos \theta_0 - \frac{Ly}{r_0} \sin \theta_0 \right)} \frac{1}{1 + \epsilon^2 (\rho_0 + \epsilon \rho_1)} \frac{\partial (p_0 + \epsilon p_1)}{\partial x}, \quad (A.48)$$

$$\epsilon \left[\frac{D(v_0 + \epsilon v_1)}{Dt} + \frac{L}{r_*} \left(\epsilon^2 (v_0 + \epsilon v_1)(w_0 + \epsilon w_1) + \left(u_0 + \epsilon u_1 \right)^2 \left(\tan \theta_0 + \frac{Ly}{r_0} \cos^{-2} \theta_0 \right) \right) \right] + (u_0 + \epsilon u_1) \frac{\left(\sin \theta_0 + \frac{Ly}{r_0} \cos \theta_0 \right)}{\sin \theta_0} = \\
= -\frac{r_0}{r_*} \frac{1}{1 + \epsilon^2 (\rho_0 + \epsilon \rho_1)} \frac{\partial (p_0 + \epsilon p_1)}{\partial y}, \quad (A.49)$$

$$\left(1 + \epsilon^2(\rho_0 + \epsilon \rho_1)\right) \left[\epsilon^5 \frac{D(w_0 + \epsilon w_1)}{Dt} - \frac{\epsilon^3 L}{r_*} \left((u_0 + \epsilon u_1)^2 + (v_0 + \epsilon v_1)^2 \right) + \right. \\
\left. - \epsilon^2 (u_0 + \epsilon u_1) \frac{\left(\cos \theta_0 - \frac{Ly}{r_0} \sin \theta_0\right)}{\sin \theta_0} \right] = \\
= -\frac{1}{\rho_s} \frac{\partial}{\partial z} \left(\rho_s(p_0 + \epsilon p_1) \right) - (\rho_0 + \epsilon \rho_1), \quad (A.50)$$

The mass continuity equation (A.40) takes the form

$$\frac{\epsilon^2 \frac{D(\rho_0 + \epsilon \rho_1)}{Dt} + \left(1 + \epsilon^2 (\rho_0 + \epsilon \rho_1)\right) \left[\frac{w_0 + \epsilon w_1}{\rho_s} \frac{\partial \rho_s}{\partial z} + \frac{\partial (w_0 + \epsilon w_1)}{\partial z} + \frac{2}{r_s} \frac{D(w_0 + \epsilon w_1)}{\partial y} - \frac{L}{r_s} (v_0 + \epsilon v_1) \left(\tan \theta_0 + \frac{Ly}{r_0} \cos^{-2} \theta_0\right) + \frac{r_0}{r_s} \frac{\cos \theta_0}{\cos \theta_0 - \frac{Ly}{r_0} \sin \theta_0} \frac{\partial (u_0 + \epsilon u_1)}{\partial x}\right] = 0. \quad (A.51)$$

If we note that $\mathcal{O}\left(\frac{D}{r_*}\right) < \mathcal{O}(\epsilon^2)$, and establish that terms of like order in ϵ must balance, we obtain, to first order,

$$\begin{cases} v_0 = \frac{\partial p_0}{\partial x}, \\ u_0 = -\frac{\partial p_0}{\partial y}, \\ \rho_0 = -\frac{1}{\rho_s} \frac{\partial}{\partial z} \left(p_0 \rho_s \right), \\ \frac{1}{\rho_s} \frac{\partial (w_0 \rho_s)}{\partial z} + \frac{\partial u_0}{\partial x} + \frac{\partial v_0}{\partial y} = 0. \end{cases}$$
(A.52)

The equation set (A.52) is the geostrophic approximation. The $\mathcal{O}(1)$ motion is thus determined by the horizontal pressure gradient. Furthermore, it can be established that the $\mathcal{O}(1)$ geostrophic velocities are horizontally nondivergent, since

$$\frac{\partial v_0}{\partial y} + \frac{\partial u_0}{\partial x} = 0, \tag{A.53}$$

which implies that

$$\frac{\partial}{\partial z}(\rho_s w_0) = 0. (A.54)$$

Hence, $\rho_s w_0$ is independent of z and if $w_0 = 0$ for any z, it will be zero $\forall z$, e.g., if the domain is bounded below or above. Thus, the vertical velocity is given by

$$w(x, y, z, t) = \epsilon w_1(x, y, z, t) + \epsilon^2 w_2(x, y, z, t) + \dots$$
 (A.55)

which is a direct consequence of the geostrophic approximation. Therefore, we cannot determine p_0 and hence u_0 and v_0 without considering higher order dynamics. The $\mathcal{O}(\epsilon)$ terms with the use of (A.55) are given below, starting with the zonal component

$$\frac{Du_0}{Dt} - \frac{Ly}{\epsilon r_0} v_0 \cot \theta_0 - v_1 = -\frac{\partial p_1}{\partial x} - \frac{Ly}{\epsilon r_0} \tan \theta_0 \frac{\partial p_0}{\partial x}, \tag{A.56}$$

where the second term on the right hand side was obtained by a little manipulation;

$$-\frac{r_0}{r_*} \frac{\cos \theta_0}{\cos \theta_0 - \frac{Ly}{r_0} \sin \theta_0} \frac{\partial p_0}{\partial x} =$$

$$= -\frac{r_0}{r_*} \frac{\cos \theta_0 \left(\cos \theta_0 + \frac{Ly}{r_0} \sin \theta_0\right)}{\left(\cos \theta_0 - \frac{Ly}{r_0} \sin \theta_0\right) \left(\cos \theta_0 + \frac{Ly}{r_0} \sin \theta_0\right)} \frac{\partial p_0}{\partial x} =$$

$$= -\frac{r_0}{r_*} \frac{\cos^2 \theta_0 + \frac{Ly}{r_0} \cos \theta_0 \sin \theta_0}{\cos^2 \theta_0 - \left(\frac{L}{r_0}\right)^2 y^2 \sin^2 \theta_0} \frac{\partial p_0}{\partial x} \approx \frac{L}{r_*} y \tan \theta_0 \frac{\partial p_0}{\partial x} \quad Q.E.D. \quad (A.57)$$

The meridional $\mathcal{O}(\epsilon)$ component is given by

$$\frac{Dv_0}{Dt} + u_0 \frac{Ly}{\epsilon r_0} \cot \theta_0 + u_1 = -\frac{\partial p_1}{\partial y}.$$
 (A.58)

The total derivative is given by

$$\frac{D}{Dt} = \frac{\partial}{\partial t} + (u_0 + \epsilon u_1) \frac{r_0}{r_*} \frac{\cos \theta_0}{\cos \theta_0 - \frac{Ly}{r_0} \sin \theta_0} \frac{\partial}{\partial x} + (v_0 + \epsilon v_1) \frac{r_0}{r_*} \frac{\partial}{\partial y} + \epsilon w_1 \frac{\partial}{\partial z}, \quad (A.59)$$

so that (A.56) and (A.58) become

$$\begin{cases}
\frac{\partial u_0}{\partial t} + u_0 \frac{\partial u_0}{\partial x} + v_0 \frac{\partial u_0}{\partial y} - v_1 - v_0 \frac{Ly}{\epsilon r_0} \cot \theta_0 = -\frac{\partial p_1}{\partial x} - \frac{Ly}{\epsilon r_0} \tan \theta_0 \frac{\partial p_0}{\partial x}, \\
\frac{\partial v_0}{\partial t} + u_0 \frac{\partial v_0}{\partial x} + v_0 \frac{\partial v_0}{\partial y} + u_1 + u_0 \frac{Ly}{\epsilon r_0} \cot \theta_0 = -\frac{\partial p_1}{\partial y}.
\end{cases}$$
(A.60)

We complete with the mass continuity equation:

$$\frac{1}{\rho_s} \frac{\partial}{\partial z} (\rho_s w_1) + \frac{\partial u_1}{\partial x} + \frac{\partial v_1}{\partial y} - v_0 \frac{L}{\epsilon r_0} \tan \theta_0 + \frac{Ly}{\epsilon r_0} \tan \theta_0 \frac{\partial u_0}{\partial x} = 0.$$
 (A.61)

Pedlosky (1987) discusses the presence of terms that are $\sim \frac{L}{\epsilon r_0}$ in the momentum equation (A.60), and notes that these terms on the left hand side are due to the variation of the Coriolis parameter on a β -plane whereas on the right hand side, these terms reflect the variation of the metric term $\cos \theta$. If $\tan \theta_0$ would be small, this term would be negligible. Then (A.60) would reduce to the $\mathcal{O}(\epsilon)$ momentum equation for a flat Earth with a linearly varying Coriolios parameter in the meridional direction. However, this would push the domain to latitudes near the equator, where the theory fails. Thus, a model of a flat Earth with sphericity accounted for only by a varying f is not valid for the $\mathcal{O}(\epsilon)$ momentum balance. Pedlosky (1987) states however, that the β -plane approximation only requires that the vorticity equation satisfies the β -plane approximation. By taking $-\frac{\partial}{\partial y}$ (A.60 a) $+\frac{\partial}{\partial x}$ (A.60 b), and noting that the relative vorticity is given by

$$\zeta_0 = \frac{\partial v_0}{\partial x} - \frac{\partial u_0}{\partial y},\tag{A.62}$$

we yield after some simplification that

$$\begin{split} \frac{\partial \zeta_0}{\partial t} + u_0 \frac{\partial \zeta_0}{\partial x} + v_0 \frac{\partial \zeta_0}{\partial y} + \left(\frac{\partial u_1}{\partial x} + \frac{\partial v_1}{\partial y} \right) + v_0 \frac{L}{\epsilon r_0} \cot \theta_0 = \\ &= \frac{L}{\epsilon r_0} \tan \theta_0 \frac{\partial p_0}{\partial x} + \frac{Ly}{\epsilon r_0} \tan \theta_0 \frac{\partial^2 p_0}{\partial x \partial y}, \quad (A.63) \end{split}$$

where use have been made of the nondivergence of the $\mathcal{O}(1)$ -momentum. We can simplify this further by taking advantage of the fact that

$$\frac{1}{\beta} = \frac{U}{\beta_0 L^2} = \frac{U}{\frac{f_0}{r_0} L^2 \cot \theta_0} = \left[\frac{L}{r_0} \sim \epsilon\right] = \frac{U}{\epsilon f_0 L \cot \theta_0} = \left[\frac{U}{f_0 L} \sim \epsilon\right] = \frac{1}{\cot \theta_0},\tag{A.64}$$

upon which we obtain

$$\frac{\partial \zeta_0}{\partial t} + u_0 \frac{\partial \zeta_0}{\partial x} + v_0 \frac{\partial \zeta_0}{\partial y} + \beta v_0 = \frac{L}{\epsilon r_0} \left[\tan \theta_0 \frac{\partial p_0}{\partial x} + y \tan \theta_0 \frac{\partial^2 p_0}{\partial x \partial y} \right] - \left(\frac{\partial u_1}{\partial x} + \frac{\partial v_1}{\partial y} \right). \tag{A.65}$$

From the geostrophic approximation (A.52), the mass continuity equation (A.61) can be rewritten as

$$\frac{1}{\rho_s} \frac{\partial(\rho_s w_1}{\partial z} + \left(\frac{\partial u_1}{\partial x} + \frac{\partial v_1}{\partial y}\right) - \frac{L}{\epsilon r_0} \tan \theta_0 \frac{\partial p_0}{\partial x} - \frac{Ly}{\epsilon r_0} \tan \theta_0 \frac{\partial^2 p_0}{\partial x \partial y} = 0, \quad (A.66)$$

from which we clearly can rewrite (A.65) as

$$\frac{D_0}{Dt} \left[\zeta_0 + \beta y \right] = \frac{1}{\rho_s} \frac{\partial (\rho_s w_1)}{\partial z},\tag{A.67}$$

where

$$\frac{D_0}{Dt} \equiv \frac{\partial}{\partial t} + u_0 \frac{\partial}{\partial x} + v_0 \frac{\partial}{\partial y}.$$
 (A.68)

It is now clear that (A.67) is the vorticity equation for a flat Earth model with a linearly varying Coriolis parameter in the meridional direction. The $\mathcal{O}(1)$ velocity field is determined in terms of p_0 by the $\mathcal{O}(1)$ momentum equation so that

$$\zeta_0 = \frac{\partial^2 p_0}{\partial x^2} + \frac{\partial^2 p_0}{\partial y^2}.$$
 (A.69)

However, we still need to resolve w_1 , which requires the use of the thermodynamic equation.

A.4. Using static stability to resolve the vertical motion

To complete the derivation of the quasigeostrophic motions we need to to represent ϵw_1 in terms of the $\mathcal{O}(1)$ geostrophic fields. This will be possible by making use of the thermodynamic equation. By considering adiabatic motions, the potential temperature θ (see (A.22)), is conserved. By making use of the ideal gas law (A.23), θ can be rewritten as

$$\theta = \frac{p}{\rho R} \left(\frac{p_0}{p} \right)^{\frac{R}{c_p}} \Longleftrightarrow \rho = \frac{p}{R\theta} \left(\frac{p_0}{p} \right)^{\frac{R}{c_p}} = \frac{p}{R\theta} \left(\frac{p}{p_0} \right)^{\frac{1}{\gamma}}, \tag{A.70}$$

where

$$\gamma \equiv \frac{c_p}{c_n}.\tag{A.71}$$

If we consider vertical displacement of an air parcel between a lower level z (A) to an upper level z + dz (B), the density of parcel A will have changed by an amount

$$\Delta \rho_A = \frac{1}{\gamma} \frac{p_0}{R\theta} \left(\frac{p}{p_0}\right)^{\frac{1}{\gamma}} \frac{\partial p}{\partial z} \frac{dz}{p}.$$
 (A.72)

Hence, the new density at z + dz is thus

$$\rho_A + \Delta \rho_A = \rho_A(z) + \frac{1}{\gamma} \frac{\rho}{p} \frac{\partial p}{\partial z} dz. \tag{A.73}$$

However, the density of parcel B at z+dz in terms of the undisturbed density A had at z, is given by

$$\rho_B = \rho_A(z) + \frac{\partial \rho}{\partial z} dz. \tag{A.74}$$

The excess density of A at z + dz is

$$(\rho_A + \Delta \rho_A) - \rho_B = \left(\frac{1}{\gamma} \frac{\rho}{p} \frac{\partial p}{\partial z} - \frac{\partial \rho}{\partial z}\right) dz, \tag{A.75}$$

which causes a restoring force

$$\frac{g}{\rho} (\rho_A + \Delta \rho_A - \rho_B) = g \left(\frac{1}{\gamma} \frac{\rho}{p} \frac{\partial p}{\partial z} - \frac{\partial \rho}{\partial z} \right) dz =
= g \left[\frac{1}{\gamma p} \frac{\partial p}{\partial z} - \frac{R\theta}{p_0} \left(\frac{p}{p_0} \right)^{-\frac{1}{\gamma}} \frac{\partial}{\partial z} \left(\frac{p_0}{R\theta} \left(\frac{p}{p_0} \right)^{\frac{1}{\gamma}} \right) \right] dz =
= g \left[\frac{1}{\gamma p} \frac{\partial p}{\partial z} - \frac{R\theta}{p_0} \left(\frac{p}{p_0} \right)^{-\frac{1}{\gamma}} \left(-\frac{1}{\theta^2} \frac{\partial \theta}{\partial z} \left(\frac{p}{p_0} \right)^{\frac{1}{\gamma}} \frac{p_0}{R} + \frac{p_0}{\gamma \theta p R} \left(\frac{p}{p_0} \right)^{\frac{1}{\gamma}} \frac{\partial p}{\partial z} \right) \right] dz =
= g \left(\frac{1}{\theta} \frac{\partial \theta}{\partial z} \right) dz \quad (A.76)$$

Thus, if $\frac{\partial \theta}{\partial z} > 0$, the buoyancy force is restoring and the static state is stable with respect to small adiabatic displacements. The static stability is defined as

$$\sigma = \frac{1}{\theta} \frac{\partial \theta}{\partial z},\tag{A.77}$$

and the fluid parcel oscillation frequency is defined by

$$N \equiv \left(\frac{g}{\theta} \frac{\partial \theta}{\partial z}\right)^{\frac{1}{2}},\tag{A.78}$$

which is commonly referred to as the Brunt-Väisälä frequency. From the definition of θ , it can be found that

$$\frac{1}{\theta} \frac{\partial \theta}{\partial z} = \frac{1}{T} \left[\frac{\partial T}{\partial z} + \frac{g}{c_p} \right], \tag{A.79}$$

if the hydrostatic approximation $\left(\frac{\partial p}{\partial z} = -\rho g\right)$ is used. Hence, if $\frac{\partial T}{\partial z} < 0$, the atmosphere will be statically stable as long as the lapse rate, $-\frac{\partial T}{\partial z} < \frac{g}{c_p}$. Finally we note that for the atmosphere, $N \sim \mathcal{O}(10^{-2}s^{-1})$.

Recalling (A.70), we note that (in dimensional form)

$$\ln \rho = \ln \left[\frac{p_0}{R\theta} \left(\frac{p}{p_0} \right)^{\frac{1}{\gamma}} \right] \iff$$

$$\ln \rho = \ln \left(\frac{p_0}{R\theta} \right) + \frac{1}{\gamma} \ln \left(\frac{p}{p_0} \right) \iff$$

$$\ln \rho = \ln p_0 - \ln R - \ln \theta + \frac{1}{\gamma} \ln p - \frac{1}{\gamma} \ln p_0 \iff$$

$$\ln \theta = \frac{1}{\gamma} \ln p - \ln \rho + \left(1 - \frac{1}{\gamma} \right) \ln p_0 - \ln R \iff \left[\gamma = \frac{c_p}{c_v} \; ; \; c_p = c_v + R \right] \iff$$

$$\ln \theta = \frac{1}{\gamma} \ln p - \ln \rho + C, \quad (A.80)$$

where

$$C = \frac{R}{c_p} \ln p_0 - \ln R. \tag{A.81}$$

Nondimensionalizing (A.80), by the use of (A.30) and (A.31), we obtain

$$\ln \theta_* = \frac{1}{\gamma} \ln \left(p_s + \rho_s U f_0 L p \right) - \ln \left[\rho_s \left(1 + \epsilon F \rho \right) \right] + C =$$

$$= \frac{1}{\gamma} \ln \left[p_s \left(1 + \frac{\rho_s U f_0 L p}{p_s / r h o_s} \right) \right] - \ln \rho_s - \ln \left(1 + \epsilon F \rho \right) + C =$$

$$= \frac{1}{\gamma} \ln p_s + \frac{1}{\gamma} \ln \left[1 + \frac{U f_0 L p}{p_s / \rho_s} \right] - \ln \rho_s - \ln \left(1 + \epsilon F \rho \right) + C =$$

$$= \frac{1}{\gamma} \ln p_s - \ln \rho_s + \frac{1}{\gamma} \ln \left[1 + \epsilon \frac{f_0^2 L^2}{p_s / \rho_s} p \right] - \ln \left(1 + \epsilon F \rho \right) + C \approx$$

$$[Taylor series expansion] \approx \frac{1}{\gamma} \ln p_s - \ln \rho_s + \epsilon \frac{1}{\gamma} \frac{f_0^2 L^2}{p_s / \rho_s} p - \epsilon F \rho + O(\epsilon^2) + C. \tag{A.82}$$

By setting

$$\ln \theta_* = \theta_s \left[1 + \epsilon F \theta(x, y, z, t) \right], \tag{A.83}$$

where

$$ln\theta_s = \frac{1}{\gamma} \ln p_s - \ln \rho_s + C, \tag{A.84}$$

and expanding θ in an ϵ -series

$$\theta = \theta_0 + \epsilon \theta_1 + \epsilon^2 \theta_2 + \dots \tag{A.85}$$

(A.82) becomes

$$\ln\left[\theta_{s}(1+\epsilon F(\theta_{0}+\epsilon\theta_{1}))\right] = \frac{1}{\gamma}\ln p_{s} - \ln \rho_{s} + \epsilon \frac{1}{\gamma} \frac{f_{0}^{2}L^{2}}{p_{s}/\rho_{s}}(p_{0}+\epsilon p_{1}) - \epsilon F(\rho_{0}+\epsilon\rho_{1}) \iff \ln \theta_{s} - \epsilon F(\theta_{0}+\epsilon\theta_{1}) \approx \frac{1}{\gamma}\ln p_{s} - \ln \rho_{s} + \epsilon \frac{1}{\gamma} \frac{f_{0}^{2}L^{2}}{p_{s}/\rho_{s}}(p_{0}+\epsilon p_{1}) - \epsilon F(\rho_{0}+\epsilon\rho_{1}) \Rightarrow F\theta_{0} = \frac{1}{\gamma} \frac{f_{0}^{2}L^{2}}{p_{s}/\rho_{s}}p_{0} - F\rho_{0}. \quad (A.86)$$

Since

$$F = \frac{f_0^2 L^2}{gD},\tag{A.87}$$

we yield

$$\theta_0 = \frac{1}{\gamma} \left(\frac{\rho_s g D}{p_s} \right) p_0 - \rho_0. \tag{A.88}$$

From the hydrostatic and geostrophic approximation, we can rewrite θ_0 as

$$\theta_0 = -\frac{p_0}{\gamma p_s} \frac{\partial p_s}{\partial z} + \frac{1}{\rho_s} \frac{\partial}{\partial z} (\rho_s p_0) = \frac{\partial p_0}{\partial z} + \frac{p_0}{\rho_s} \frac{\partial \rho_s}{\partial z} - \frac{p_0}{\gamma p_s} \frac{\partial p_s}{\partial z}. \tag{A.89}$$

By noting that (A.84) is equivalent to

$$\theta_{s} = \frac{p_{s}^{\frac{1}{\gamma}}}{\rho_{s}} + C \Rightarrow \frac{\partial \theta_{s}}{\partial z} = \frac{\partial}{\partial z} \left(\frac{p_{s}^{\frac{1}{\gamma}}}{\rho_{s}} \right) \Rightarrow \dots \Rightarrow \frac{1}{\theta_{s}} \frac{\partial \theta_{s}}{\partial z} = \frac{1}{\gamma p_{s}} \frac{\partial p_{s}}{\partial z} - \frac{1}{\rho_{s}} \frac{\partial \rho_{s}}{\partial z}, \tag{A.90}$$

we can rewrite θ_0 as

$$\theta_0 = \frac{\partial p_0}{\partial z} - p_0 \frac{1}{\theta_s} \frac{\partial \theta_s}{\partial z}.$$
 (A.91)

However, if we make use of the observation that

$$\frac{1}{\theta_s} \frac{\partial \theta_s}{\partial z} \sim \mathcal{O}(\epsilon), \tag{A.92}$$

we obtain

$$\theta_0 = \frac{\partial p_0}{\partial z}.\tag{A.93}$$

Now, let us invoke (A.83) into the thermodynamic equation (A.21), i.e.,

$$\begin{split} \frac{D\theta_*}{Dt_*} &= \frac{\theta}{c_p T_*} \left(\frac{k}{\rho_*} \nabla^2 T_* + Q_* \right) \Longleftrightarrow \\ \frac{D\theta_s (1 + \epsilon F(\theta_0 + \epsilon \theta_1))}{D \left(\frac{L}{U} t \right)} &= \frac{\theta_s (1 + \epsilon F(\theta_0 + \epsilon \theta_1))}{c_p T} \left(\frac{k}{\rho_*} \nabla^2 T_* + Q_* \right) \Longleftrightarrow \\ \frac{U}{L} \left[\frac{D\theta_s}{Dt} (1 + \epsilon F(\theta_0 + \epsilon \theta_1)) + \theta_s \epsilon F \frac{D(\theta_0 + \epsilon \theta_1)}{dt} \right] &= \\ &= \frac{\theta_s (1 + \epsilon F(\theta_0 + \epsilon \theta_1))}{c_p T} \left(\frac{k}{\rho_*} \nabla^2 T_* + Q_* \right) \Longleftrightarrow \\ \frac{D\theta}{Dt} + \frac{w(1 + \epsilon F\theta)}{\epsilon F\theta_s} \frac{\partial \theta_s}{\partial z} &= \left[\epsilon = \frac{U}{f_0 L} \; ; \; F = \frac{f_0^2 L^2}{g D} \right] = \frac{\theta_*}{\theta_s} \left(\frac{\kappa_*}{c_p T_*} \right) \frac{g D}{U^2 f_0}, \end{split}$$
(A.94)

where

$$\kappa_* \equiv \frac{k}{\rho_*} \nabla^2 T_* + Q_*. \tag{A.95}$$

Pedlosky (1987) notes that for the atmosphere, $c_pT_* \sim \mathcal{O}(gD) \Rightarrow \kappa_* \leq \mathcal{O}(U^2f_0)$ and so we nondimensionalize κ_* as

$$\kappa = \kappa * \frac{gD}{c_n T_* f_0 U^2}.$$
 (A.96)

Since the vertical velocity can be expressed as $w = \epsilon w_1 + \epsilon^2 w_2 + ...$, we rewrite (A.94) as

$$\frac{\partial(\theta_0 + \epsilon \theta_1)}{\partial t} + (u_0 + \epsilon u_1) \frac{\partial(\theta_0 + \epsilon \theta_1)}{\partial x} + (v_0 + \epsilon v_1) \frac{\partial(\theta_0 + \epsilon \theta_1)}{\partial y} + \frac{(w_1 + \epsilon w_2)}{F\theta_s} \frac{\partial \theta_s}{\partial z} (1 + \epsilon F(\theta_0 + \epsilon \theta_1)) = (1 + \epsilon F(\theta_0 + \epsilon \theta_1))\kappa. \quad (A.97)$$

Thus, to lowest order we have

$$\frac{D\theta_0}{Dt} + w_1 \frac{1}{F\theta_s} \frac{\partial \theta_s}{\partial z} = \kappa. \tag{A.98}$$

We now define the stratification parameter, S(z), as

$$S(z) = \frac{1}{F\theta_s} \frac{\partial \theta_s}{\partial z} = \frac{N_s^2 D^2}{f_0^2 L^2} \sim \mathcal{O}(1), \tag{A.99}$$

and

$$N_s^2 = \frac{g}{D\theta_s} \frac{\partial \theta_s}{\partial z}.$$
 (A.100)

The heating rate κ can be considered small over the advective time scale, but in general, the $O(\epsilon)$ vertical motion is obtained from

$$w_1 = \left[\kappa - \frac{D_0 \theta_0}{Dt}\right] \frac{1}{S(z)}.$$
 (A.101)

Hence, the vertical velocity is now described by the $\mathcal{O}(1)$ dynamical θ_0 -field and can be substituted into the right hand side of (A.67) to yield

$$\frac{1}{\rho_s} \frac{\partial(\rho_s w_1)}{\partial z} = \frac{1}{\rho_s} \frac{\partial}{\partial z} \left[\frac{\rho_s}{S(z)} \left(\kappa - \frac{D_0 \theta_0}{Dt} \right) \right] =
= \frac{1}{\rho_s} \frac{\partial}{\partial z} \left[\frac{\rho_s \kappa}{S(z)} \right] - \frac{1}{\rho_s} \frac{D_0}{Dt} \left[\frac{\partial}{\partial z} \left(\frac{\rho_s}{S(z)} \theta_0 \right) \right] + \frac{1}{S(z)} \left(\frac{\partial u_0}{\partial z} \frac{\partial \theta_0}{\partial x} + \frac{\partial v_0}{\partial z} \frac{\partial \theta_0}{\partial y} \right).$$
(A.102)

From the geostrophic approximation (A.52) and the hydrostatic approximation (A.93) the thermal wind relation can be established;

$$\begin{cases}
\frac{\partial v_0}{\partial z} = \frac{\partial \theta_0}{\partial x}, \\
\frac{\partial u_0}{\partial z} = -\frac{\partial \theta_0}{\partial y}.
\end{cases}$$
(A.103)

upon which the last term in (A.102) identically vanish. Thus, the vorticity equation (A.67) reduces to

$$\frac{D_0}{Dt} \left[\zeta_0 + \beta y + \frac{1}{\rho_s} \frac{\partial}{\partial z} \left(\frac{\rho_s(z)}{S(z)} \theta_0 \right) \right] = \frac{1}{\rho_s} \frac{\partial}{\partial z} \left[\frac{\rho_s(z)\kappa}{S(z)} \right]. \tag{A.104}$$

In the absence of a heating source, we can neglect the right hand side and thus obtain a conservation statement

$$\frac{D_0}{Dt} \left[\zeta_0 + \beta y + \frac{1}{\rho_s} \frac{\partial}{\partial z} \left(\frac{\rho_s(z)}{S(z)} \theta_0 \right) \right] = 0, \tag{A.105}$$

or, equivalently,

$$\frac{D_0 q}{Dt} = 0, (A.106)$$

where

$$q = \zeta_0 + \beta y + \frac{1}{\rho_s} \frac{\partial}{\partial z} \left(\frac{\rho_s(z)}{S(z)} \theta_0 \right). \tag{A.107}$$

The geostrophic and hydrostatic approximations allow us to express each dependent variable as $p_0 = \psi$, whereupon

$$\left[\frac{\partial}{\partial t} - \frac{\partial \psi}{\partial y}\frac{\partial}{\partial x} + \frac{\partial \psi}{\partial x}\frac{\partial}{\partial y}\right]\left[\frac{\partial^2 \psi}{\partial x^2} + \frac{\partial^2 \psi}{\partial y^2} + \frac{1}{\rho_s}\frac{\partial}{\partial z}\left(\frac{\rho_s(z)}{S(z)}\frac{\partial \psi}{\partial z}\right) + \beta y\right] = 0.$$
(A.108)

This is the governing equation of motion for a stratified fluid, the so-called quasi-geostrophic potential vorticity equation for a homogeneous layer of fluid. It is completely written in terms of the $\mathcal{O}(1)$ pressure field or stream function. Once it has been determined, u_0 , v_0 , ρ_0 , θ_0 and w_1 follow directly.

A.6. Connecting the QGPV equation to Charney's theory

Charney (1971) derived an original theory on geostrophic turbulence following the conservation of the quantity he denoted pseudo-potential vorticity. The aim is to link (A.108) to Charney's theory. We start by noting that (A.108) can be written as

$$\frac{D_0}{Dt} \left[\nabla_H^2 \psi + \beta y + \frac{1}{\rho_s} \frac{\partial}{\partial z} \left(\frac{\rho_s(z)}{S(z)} \frac{\partial \psi}{\partial z} \right) \right] = 0, \tag{A.109}$$

and that

$$S(z) = \frac{1}{F\theta_s} \frac{\partial \theta_s}{\partial z} = \frac{N_s^2 D^2}{f_0^2 L^2},$$
 (A.110)

which hence leads to

$$\frac{D_0}{Dt} \left[\nabla_H^2 \psi + \beta y + \frac{1}{\rho_s} \frac{\partial}{\partial z} \left(\frac{f_0^2 L^2}{N_s^2 D^2} \rho_s \frac{\partial \psi}{\partial z} \right) \right] = 0. \tag{A.111}$$

Expansion of the third term in (A.111) yields

$$\frac{1}{\rho_s} \frac{\partial}{\partial z} \left(\frac{f_0^2 L^2}{N_s^2 D^2} \rho_s \frac{\partial \psi}{\partial z} \right) = \frac{f_0^2 L^2}{N_s^2 D^2} \left(\frac{\partial^2 \psi}{\partial z^2} + \frac{1}{\rho_s} \frac{\partial \rho_s}{\partial z} \frac{\partial \psi}{\partial z} - \frac{2}{N_s} \frac{\partial N_s}{\partial z} \frac{\partial \psi}{\partial z} \right), \tag{A.112}$$

so that

$$\frac{D_0}{Dt} \left[\nabla_H^2 \psi + \frac{f_0^2 L^2}{N_s^2 D^2} \left(\frac{\partial^2 \psi}{\partial z^2} + \frac{1}{\rho_s} \frac{\partial \rho_s}{\partial z} \frac{\partial \psi}{\partial z} - \frac{2}{N_s} \frac{\partial N_s}{\partial z} \frac{\partial \psi}{\partial z} \right) \right] + \beta \frac{\partial \psi}{\partial x} = 0.$$
(A.113)

Introducing the Charney substitution

$$\psi = \left(\frac{\rho_0}{\rho_s}\right)^n \chi,\tag{A.114}$$

which is inserted into (A.113) to yield, after a little simplification,

$$\frac{D_0}{Dt} \left[\left(\frac{\rho_0}{\rho_s} \right)^n \nabla_H^2 \chi + \rho_0^n \frac{f_0^2 L^2}{N_s^2 D^2} \left[\frac{\partial \rho_s}{\partial z} \chi \left(\rho_s^{-n-1} \frac{2n}{N_s} \frac{\partial N_s}{\partial z} + \rho_s^{-n-2} n^2 \left(\frac{\partial \rho_s}{\partial z} \right)^2 \right) + \right. \\
\left. - n \rho_s^{-n-1} \frac{\partial^2 \rho_s}{\partial z^2} \chi - \rho_s^{-n} \frac{2}{N_s} \frac{\partial N_s}{\partial z} \frac{\partial \chi}{\partial z} + \rho_s^{-n-1} \left(1 - 2n \right) \frac{\partial \rho_s}{\partial z} \frac{\partial \chi}{\partial z} + \rho_s^{-n} \frac{\partial^2 \chi}{\partial z^2} \right] \right] + \\
+ \beta \left(\frac{\rho_0}{\rho_s} \right)^n \frac{\partial \chi}{\partial x} = 0. \quad (A.115)$$

Choosing $n = \frac{1}{2}$, we yield a convenient cancellation of the second term involving $\frac{\partial \chi}{\partial z}$. Rescaling the vertical coordinate as

$$\begin{cases}
\frac{\partial}{\partial z} \to \frac{N_s D}{f_0 L} \frac{\partial}{\partial Z}, \\
\frac{\partial^2}{\partial z^2} \to \frac{N_s^2 D^2}{f_0^2 L^2} \frac{\partial^2}{\partial Z^2} + \frac{N_s^2 D^2}{f_0^2 L^2} \frac{1}{N_s} \frac{\partial N_s}{\partial Z} \frac{\partial}{\partial Z},
\end{cases} (A.116)$$

we obtain, after multiplication by $\left(\frac{\rho_s}{\rho_0}\right)^{\frac{1}{2}}$ and using $n=\frac{1}{2}$,

$$\frac{D_0}{Dt} \left[\nabla_H^2 \chi + \frac{1}{4\rho_s^2} \left(\frac{\partial \rho_s}{\partial Z} \right)^2 \chi - \frac{1}{2\rho_s} \frac{\partial^2 \rho_s}{\partial Z^2} \chi + \frac{1}{2\rho_s} \frac{\partial \ln N_s}{\partial Z} \frac{\partial \rho_s}{\partial Z} \chi \right. \\
\left. - \frac{\partial \ln N_s}{\partial Z} \frac{\partial \chi}{\partial Z} + \frac{\partial^2 \chi}{\partial Z^2} \right] + \beta \frac{\partial \chi}{\partial x} = 0. \quad (A.117)$$

Assuming that the atmospheric density profile can be approximated as (for example, this choice is arbitrary and does not influence the validity of the theory);

$$\rho_s = \rho_0 e^{-\frac{f_0 L}{DN_s} Z},\tag{A.118}$$

we obtain

$$\frac{D_0}{Dt} \left[\nabla_3^2 \chi - \frac{\partial \ln N_s}{\partial z} \left(\frac{\partial \chi}{\partial Z} + \frac{1}{2} \frac{f_0 L}{N_s D} \chi \right) - \frac{1}{4} \frac{f_0^2 L^2}{N_s^2 D^2} \chi \right] + \beta \frac{\partial \chi}{\partial x} = 0. \quad (A.119)$$

Introducing the internal Rossby deformation radius

$$\lambda = \frac{N_s D}{f_0},\tag{A.120}$$

this can be simplified to

$$\frac{D_0}{Dt} \left[\nabla_3^2 \chi - \frac{\partial \ln N_s}{\partial z} \left(\frac{\partial \chi}{\partial Z} + \frac{L}{2\lambda} \chi \right) - \frac{L^2}{4\lambda^2} \chi \right] + \beta \frac{\partial \chi}{\partial x} = 0.$$
 (A.121)

A comparison with Charney (1971) shows that the governing equations are exactly the same except from the presence of the potential temperature θ instead of N_s . It is likely that this is just a typo in Charney (1971), which is supported by the subsequent assumption that the scale of variation of N_s is larger than the vertical scale of the turbulence, upon which terms involving the vertical gradient of N_s are neglected. Note however, that the assumption that the vertical scale of variation of lnN_s is smaller than the vertical scale of the turbulence, is a weaker assumption. In addition, Charney neglected the β -term by noting that advection of relative vorticity dominates over the advection of the Earth's vorticity. Charney also made the assumption that $\mathcal{O}(L) < \mathcal{O}(2\lambda)$ and hence neglected the potential term. However, we will keep both the potential and the β -term in the following. Thus,

$$\frac{D_0}{Dt} \left[\nabla_3^2 \chi - \frac{L^2 \chi}{4\lambda^2} \right] + \beta \frac{\partial \chi}{\partial x} \approx 0.$$
 (A.122)

where the total derivative is given by

$$\frac{D_0}{Dt} = \frac{\partial}{\partial t} + e^{\frac{L}{2\lambda}Z} \left(\frac{\partial \chi}{\partial x} \frac{\partial}{\partial y} - \frac{\partial \chi}{\partial y} \frac{\partial}{\partial x} \right)$$
(A.123)

where use have been made of (A.114) and (A.118). Since Charney assumed that $\mathcal{O}(L) < \mathcal{O}(2\lambda)$, the exponential term multiplying the advective operator vanishes. However, it might be interesting to note that the case $\mathcal{O}(L) \gtrsim \mathcal{O}(2\lambda)$ can be accomodated for by scaling the time as

$$t \to e^{-\frac{L}{2\lambda}Z}\tau,\tag{A.124}$$

so to yield

$$\frac{D_0}{D\tau} = \frac{\partial}{\partial \tau} + \left(\frac{\partial \chi}{\partial x}\frac{\partial}{\partial y} - \frac{\partial \chi}{\partial y}\frac{\partial}{\partial x}\right). \tag{A.125}$$

It is noteworthy that this implies that the non-dimensional time now scale with height, which is a scenario that has not been explored to the best of the author's knowledge.

We now wish to examine the time evolution of energy and enstrophy. By multiplying (A.122) by $\rho_s \chi$ we obtain

$$\rho_s \chi \left[\frac{\partial}{\partial \tau} + \left(\frac{\partial \chi}{\partial x} \frac{\partial}{\partial y} - \frac{\partial \chi}{\partial y} \frac{\partial}{\partial x} \right) \right] \left[\nabla_3^2 \chi - \frac{L^2 \chi}{4\lambda^2} \right] = 0.$$
 (A.126)

The first term can be rewritten as

$$\rho_s \chi \frac{\partial}{\partial \tau} \left[\nabla_3^2 \chi - \frac{L^2 \chi}{4\lambda^2} \right] = \rho_s \chi \nabla_3^2 \frac{\partial \chi}{\partial \tau} - \rho_s \frac{L^2}{4\lambda^2} \chi \frac{\partial \chi}{\partial \tau}. \tag{A.127}$$

Omitting the subscript 3 for the three-dimensional Laplacian and noting that

$$\begin{cases}
\nabla \cdot \left[\chi \nabla \frac{\partial \chi}{\partial \tau} \right] = \chi \nabla^2 \frac{\partial \chi}{\partial \tau} + \nabla \chi \cdot \nabla \frac{\partial \chi}{\partial \tau}, \\
\frac{\partial}{\partial \tau} \frac{(\nabla \chi)^2}{2} = \nabla \chi \cdot \nabla \frac{\partial \chi}{\partial \tau},
\end{cases} (A.128)$$

the first term (A.127) can be rewritten as

$$\rho_s \left(\nabla \cdot \left[\chi \nabla \frac{\partial \chi}{\partial \tau} \right] - \frac{\partial}{\partial \tau} \frac{\left(\nabla \chi \right)^2}{2} - \frac{L^2}{8\lambda^2} \frac{\partial \chi^2}{\partial \tau} \right). \tag{A.129}$$

The second term in (A.126) can be rewritten as

$$\rho_{s}\chi\left(\frac{\partial\chi}{\partial x}\frac{\partial}{\partial y} - \frac{\partial\chi}{\partial y}\frac{\partial}{\partial x}\right)\left(\nabla_{3}^{2}\chi - \frac{L^{2}\chi}{4\lambda^{2}}\right) =$$

$$= \rho_{s}\chi\left(\frac{\partial\chi}{\partial x}\frac{\partial}{\partial y}\nabla^{2}\chi - \frac{\partial\chi}{\partial y}\frac{\partial}{\partial x}\nabla^{2}\chi\right). \quad (A.130)$$

This can be reformulated by the use of the following observation;

$$\nabla \cdot \left(\boldsymbol{u} \chi \nabla^2 \chi \right) = \frac{\partial}{\partial x} \left(-\frac{\partial \chi}{\partial y} \chi \nabla^2 \chi \right) + \frac{\partial}{\partial y} \left(\frac{\partial \chi}{\partial x} \chi \nabla^2 \chi \right) = \dots = \chi \left(\boldsymbol{u} \cdot \nabla \right) \nabla^2 \chi, \tag{A.131}$$

upon which (A.126) can be written as

$$\rho_s \frac{\partial}{\partial \tau} \left[\frac{(\nabla \chi)^2}{2} + \frac{L^2}{8\lambda^2} \chi^2 \right] - \rho_s \nabla \cdot \left[\boldsymbol{u} \chi \nabla^2 \chi + \chi \nabla \frac{\partial \chi}{\partial \tau} \right] = 0. \tag{A.132}$$

Integration of (A.132) over a normalized cubic volume L^3 yields

$$\frac{1}{L^{3}} \int \int \int \left[\rho_{s} \frac{\partial}{\partial \tau} \left[\frac{(\nabla \chi)^{2}}{2} + \frac{L^{2}}{8\lambda^{2}} \chi^{2} \right] - \right] \\
- \rho_{s} \nabla \cdot \left[\mathbf{u} \chi \nabla^{2} \chi + \chi \nabla \frac{\partial \chi}{\partial \tau} \right] \right] L dx \ L dy \ \frac{f_{0} L}{N_{s} D} dZ = const. \iff \\
\frac{\partial}{\partial \tau} \int \int \int \frac{\rho_{s}}{2\lambda} \left[(\nabla \chi)^{2} + \frac{L^{2}}{4\lambda^{2}} \chi^{2} \right] dx \ dy \ dZ + \\
- \int \int \int \frac{\rho_{s}}{\lambda} \nabla \cdot \left[\mathbf{u} \chi \nabla^{2} \chi + \chi \nabla \frac{\partial \chi}{\partial \tau} \right] dx \ dy \ dZ = const. \iff \\
\frac{\partial}{\partial \tau} \int \int \int \frac{\rho_{s}}{2\lambda} \left[(\nabla \chi)^{2} + \frac{L^{2}}{4\lambda^{2}} \chi^{2} \right] dx \ dy \ dZ - \int \int \int \frac{\rho_{s}}{\lambda} \nabla \cdot \mathbf{J} \ dx \ dy \ dZ = const. \tag{A.133}$$

Making use of the divergence theorem and multiplying by λ , this can be rewritten as

$$\frac{\partial}{\partial t} \int \int \int \frac{\rho_s}{2} \left[(\nabla \chi)^2 + \frac{L^2}{4\lambda^2} \chi^2 \right] dx dy dZ - \oiint \rho_s \mathbf{J} \cdot \hat{\mathbf{n}} dA = const. \quad (A.134)$$

The closed integral vanishes and we obtain

$$\int \int \int \frac{\rho_s}{2} \left[(\nabla \chi)^2 + \frac{L^2}{4\lambda^2} \chi^2 \right] dx \, dy \, dZ = const. \iff$$

$$\int \int \int \frac{\rho_s}{2} \left(\left[\left(\frac{\partial \chi}{\partial x} \right)^2 + \left(\frac{\partial \chi}{\partial y} \right)^2 \right] + \left[\left(\frac{\partial \chi}{\partial Z} \right)^2 + \xi^2 \chi^2 \right] \right) \, dx \, dy \, dZ = const., \tag{A.135}$$

where

$$\xi \equiv \frac{L}{2\lambda}.\tag{A.136}$$

The first bracketed term in (A.135) corresponds to the kinetic energy whereas the second bracketed term contains the available potential energy, APE. The major point here is that energy is conserved.

Now, let us examine the temporal evolution of enstrophy. We begin by

multiplying (A.122) by $(\nabla^2 \chi - \xi^2 \chi)$, thus obtaining

$$\left(\nabla^{2}\chi - \xi^{2}\chi\right) \left[\frac{\partial}{\partial \tau} + \left(\frac{\partial \chi}{\partial x}\frac{\partial}{\partial y} - \frac{\partial \chi}{\partial y}\frac{\partial}{\partial x}\right)\right] \left[\nabla^{2}\chi - \frac{L^{2}\chi}{4\lambda^{2}}\right] = 0 \iff \frac{1}{2}\frac{\partial}{\partial \tau} \left(\nabla^{2}\chi - \xi^{2}\chi\right)^{2} + \left(\nabla^{2}\chi - \xi^{2}\chi\right) \left(\frac{\partial \chi}{\partial x}\frac{\partial}{\partial y} - \frac{\partial \chi}{\partial y}\frac{\partial}{\partial x}\right) \left(\nabla^{2}\chi - \xi^{2}\chi\right) = 0. \tag{A.137}$$

The second term can be rewritten as

$$\left(\nabla^{2}\chi - \xi^{2}\chi\right) \left(\frac{\partial\chi}{\partial x}\frac{\partial}{\partial y} - \frac{\partial\chi}{\partial y}\frac{\partial}{\partial x}\right) \left(\nabla^{2}\chi - \xi^{2}\chi\right) =
= \left(\nabla^{2}\chi - \xi^{2}\chi\right) \left(\boldsymbol{u}\cdot\nabla\right) \left(\nabla^{2}\chi - \xi^{2}\chi\right) = \left[\Phi \equiv \nabla^{2}\chi - \xi^{2}\chi\right] =
= \Phi\left(\boldsymbol{u}\cdot\nabla\right)\Phi = \left(\boldsymbol{u}\cdot\nabla\right)\frac{\Phi^{2}}{2} = \dots = \nabla\cdot\boldsymbol{u}\left[\frac{1}{2}\Phi^{2}\right] \quad (A.138)$$

Thus, (A.137) can be reformulated as

$$\frac{1}{2}\frac{\partial}{\partial \tau}\Phi^2 + \nabla \cdot \boldsymbol{u} \left[\frac{1}{2}\Phi^2 \right] = 0. \tag{A.139}$$

Defining the potential enstrophy as

$$Q \equiv \frac{1}{2}\Phi^{2} = \frac{1}{2}\left(\nabla^{2}\chi - \xi^{2}\chi\right)^{2},\tag{A.140}$$

we obtain

$$\frac{\partial Q}{\partial t} + \nabla \cdot (\boldsymbol{u}Q) = 0. \tag{A.141}$$

Normalized triple integration yields

$$\frac{1}{L^{3}} \int \int \int \left(\frac{\partial Q}{\partial \tau} + \nabla \cdot (\mathbf{u}Q) \right) L dx L dy \frac{L}{\lambda} Z = const. \iff
\frac{\partial}{\partial \tau} \int \int \int \frac{1}{\lambda} Q dx dy dZ + \oiint \frac{1}{\lambda} Q \mathbf{u} \cdot \hat{\mathbf{n}} dA = const. \implies
\int \int \int Q dx dy dZ = const. \quad (A.142)$$

Thus, both energy and enstrophy are conserved within the quasigeostrophic framework when Charney assumptions have been implemented.

A.7. The role of the β -term

Up to now, we have not considered the possible role of the β -term in terms of quasigeostrophic dynamics. One way to gain further insight is to study a simplified model such as the two-layer model. It is the most basic model in which baroclinic effects are present. Following Holton (2004), we start by

looking at the quasigeostrophic potential vorticity equation, where we have restored the z-coordinate from Charney scaling.

$$\frac{\partial q}{\partial t} + (\mathbf{u_h} \cdot \nabla)q = 0, \tag{A.143}$$

where

$$q = \nabla_h^2 \psi + \lambda_d^{-2} \frac{\partial^2}{\partial z^2} \psi + f, \tag{A.144} \label{eq:A.144}$$

and

$$f = f_0 + \beta y \tag{A.145}$$

is the Coriolis parameter on a β -plane and

$$\lambda_d = \frac{ND}{f_0} \tag{A.146}$$

is the Rossby radius of deformation corresponding to a vertical scale D. We now separate the equation into two vertically separated layers so that

$$q_1 = f_0 + \beta y + \nabla_h^2 \psi_1 + \lambda_d^{-2} (\psi_2 - \psi_1), \tag{A.147}$$

and

$$q_2 = f_0 + \beta y + \nabla_h^2 \psi_2 + \lambda_d^{-2} (\psi_1 - \psi_2), \tag{A.148}$$

where 1 and 2 denotes the upper and lower layer, respectively. The barotropic (denoted m) and baroclinic (denoted t) components can be defined as

$$\begin{cases} \psi_m \equiv \frac{\psi_1 + \psi_2}{2}, \\ \psi_t \equiv \frac{\psi_1 - \psi_2}{2}, \end{cases}$$

and equivalently

$$\begin{cases} q_m \equiv \frac{q_1 + q_2}{2}, \\ q_t \equiv \frac{q_1 - q_2}{2}. \end{cases}$$

Thus, the potential vorticity equations in each layer can be rewritten as

$$q_1 = \beta y + \nabla^2 (2\psi_m - \psi_2) - 2\lambda_d^{-2} \psi_t,$$
 (A.149)

and

$$q_2 = \beta y + \nabla^2 \psi_2 + 2\lambda_d^{-2} \psi_t, \tag{A.150}$$

and hence

$$q_m = \beta y + \nabla^2 \psi_m,$$

$$q_t = \nabla^2 \psi_t - 2\lambda_d^{-2} \psi_t.$$
(A.151)
(A.152)

$$q_t = \nabla^2 \psi_t - 2\lambda_d^{-2} \psi_t. \tag{A.152}$$

At this point we note that in the midlatitude atmosphere, there is climatologically a mean zonal flow. So it is convenient to linearise the equations about a uniform mean zonal wind state so that

$$\left\{ \begin{array}{l} \psi_m = -u_m y + \psi_m', \\ \psi_t = -u_t y + \psi_t', \end{array} \right.$$

where u_m is the mean zonal wind and u_t is the mean thermal wind;

$$\begin{cases} u_m \equiv \frac{u_1 + u_2}{2}, \\ u_t \equiv \frac{u_1 - u_2}{2}. \end{cases}$$

Substitutions into the vorticity equations and linearisation (neglecting products of perturbation quantities) for each layer yield

$$\left[\frac{\partial}{\partial t} + u_1 \frac{\partial}{\partial x}\right] (q_1 + q_1') + u_1' \frac{\partial q_1}{\partial x} + v_1' \frac{\partial q_1}{\partial y} = 0, \tag{A.153}$$

$$\left[\frac{\partial}{\partial t} + u_2 \frac{\partial}{\partial x}\right] (q_2 + q_2') + u_2' \frac{\partial q_2}{\partial x} + v_2' \frac{\partial q_2}{\partial y} = 0, \tag{A.154}$$

where q_1 and q_2 are given by (A.149) and (A.150) and

$$u_1 = u_m + u_t, \tag{A.155}$$

$$u_2 = u_m - u_t. \tag{A.156}$$

Furthermore, it could be noted that

$$q_m = \beta y, \tag{A.157}$$

$$q_m' = \nabla^2 \psi_m', \tag{A.158}$$

$$q_t = 2\lambda_d^{-2} u_t y, \tag{A.159}$$

$$q_t' = \nabla^2 \psi_t' - 2\lambda_d^{-2} \psi_t'. \tag{A.160}$$

Summation, rearrangement and dropping the primes for the stream functions give eventually the evolution of the barotropic perturbation vorticity;

$$\left[\frac{\partial}{\partial t} + u_m \frac{\partial}{\partial x}\right] \nabla^2 \psi_m + \beta \frac{\partial \psi_m}{\partial x} + u_t \frac{\partial}{\partial x} \nabla^2 \psi_t = 0, \tag{A.161}$$

whereas subtraction gives the baroclinic evolution

$$\left[\frac{\partial}{\partial t} + u_m \frac{\partial}{\partial x}\right] \left(\nabla^2 \psi_t - 2\lambda_d^{-2} \psi_t\right) + \beta \frac{\partial \psi_t}{\partial x} + u_t \frac{\partial}{\partial x} \left(\nabla^2 \psi_m + 2\lambda_d^{-2} \psi_m\right) = 0.$$
(A.162)

In the simplest case, we study wave-like solutions of the form

$$\psi_m = Ae^{ik(x-ct)},\tag{A.163}$$

$$\psi_t = Be^{ik(x-ct)},\tag{A.164}$$

which we substitute into (A.161) and (A.162) upon which we obtain (after dividing through by the exponential factors) a set of linear equations for the coefficients:

$$ik\left[(c-u_m)k^2+\beta\right]A-ik^3u_tB=0, \tag{A.165}$$

$$ik\left[(c-u_m)(k^2+2\lambda_d^{-2})+\beta\right]B-iku_t(k^2-2\lambda_d^{-2})A=0,$$
 (A.166)

which gives us nontrivial solutions only if the determinant is zero and hence we obtain a dispersion relation for c:

$$(c - u_m)^2 k^2 (k^2 + 2\lambda_d^{-2}) + 2(c - u_m)\beta(k^2 + \lambda_d^{-2}) + \beta^2 + u_t^2 k^2 (2\lambda_d^{-2} - k^2) = 0,$$
(A.167)

from which the phase speed can be obtained as (see Holton, 2004):

$$c = u_m - \frac{\beta(k^2 + \lambda_d^{-2})}{k^2(k^2 + 2\lambda_d^{-2})} \pm \delta^{\frac{1}{2}}, \tag{A.168}$$

where

$$\delta = \frac{\beta^2 \lambda_d^{-4}}{k^4 (k^2 + 2\lambda_d^{-2})^2} - \frac{u_t^2 (2\lambda_d^{-2} - k^2)}{k^2 + 2\lambda_d^{-2}}.$$
 (A.169)

It is immediately apparent that if $\delta < 0$, we will obtain solutions that grow in time. If we consider the case when $\beta = 0$, we find that $\delta < 0$ if $k^2 < 2\lambda_d^{-2}$. Thus, we can conclude that long waves are sensitive to perturbations and will tend to grow with time. Furthermore, a greater Rossby radius decreases the critical wave number (towards larger scales) at which perturbations start to grow according to this simple model. Recalling what the deformation radius actually tells us,

$$\lambda_d = \frac{ND}{f_0},\tag{A.170}$$

we can see that an increase in static stability or tropospheric depth act to constrain the perturbation growth to larger scales, whereas an increase in the rotation rate decreases the Rossby radius and so acts to excite modes at higher wavenumbers. The main question of this chapter is the role of the β -effect. Already in (A.169) it is clear that for $\beta > 0$ and everything but the thermal wind kept constant, the role of the β -effect is to stabilize the flow. Thus, for perturbations to grow, the vertical wind shear (reflected in u_t) must increase for instabilities to develop. Exploiting (A.169) to analyse this in more detail, we set up the condition $\delta < 0$ and simplify the equation so to yield

$$k^4 < 2\lambda_d^{-2} \pm \sqrt{4\lambda_d^{-8} - \frac{\beta^2 \lambda_d^{-4}}{u_t^2}},$$
 (A.171)

which gives rise to complex solutions if $u_t > \frac{\beta \lambda_d^2}{2}$. Thus, it is evident that the β -effect acts to stabilize the flow, since the criticial vertical wind shear needed increases when β increases. It is also noteworthy that in the absence of a vertical wind shear we only yield free oscillations upon a barotropic flow with a phase speed for the barotropic perturbation that corresponds to that for a barotropic Rossby wave, i.e.,

$$c = u_m - \frac{\beta}{k^2}. (A.172)$$

How is the β -effect expected to manifest itself in our simulations? According to Vallis (2006), we could expect an inverse energy transfer that is deflected into the $k_x=0$ -mode so that the flow becomes more zonal. We could also, depending on the strength of the β -effect and hence at which length-scales its presence are felt, expect Rossby waves to develop. Thus, if there is a wide enough region in k-space between the so-called Rhines scale and the scale at which the friction dominates, waves would dominate the flow rather than geostrophic turbulence itself, in this particular region.

Bibliography

- Bartello, P. and Warn, T. 1996 Self-similarity of decaying two-dimensional turbulence J. Fluid Mech., 326, 357.
- Batchelor, G. K. 1969 Computation of the energy spectrum in homogeneous twodimensional turbulence *Phys. Fluids Suppl. II*, **12**, 233.
- Boffetta, G., Celani, A. and Vergassola, M. 2000 Inverse energy cascade in two-dimensional turbulence: deviations from Gaussian behavior *Phys. Rev. E.*, **61**, 29.
- BOFFETTA, G. 2007 Energy and enstrophy fluxes in the double cascade of twodimensional turbulence J. Fluid Mech., **589**, 253.
- VAN BOKHOVEN, L. J. A., TRIELING, R. R., CLERCX, H. J. H. AND VAN HEIJST, G. J. F. 2007 Influence of initial conditions on decaying two-dimensional turbulence *Phys. Fluids*, **19**, 046601.
- BORUE, V. 1994 Inverse energy cascade in stationary two-dimensional homogeneous turbulence *Phys. Rev. L.*, **72**, 1475.
- Bracco, A. and McWilliams, J. 2010 Reynolds-number dependency in homogeneous, stationary two-dimensional turbulence *J. Fluid Mech.*, accepted.
- CARNEVALE, G. F., McWilliams, J. C., Pomeau, Y., Weiss, J. B. and Young, W. R. 1991 Evolution of vortex statistics in two-dimensional turbulence *Phys. Rev. L.*, **66**, 2735.
- Charney, J. G. 1971 Geostrophic turbulence J. Atm. Sci., 28, 1087.
- Danilov, S. D. and Gurarie, D. 2000 Quasi-two-dimensional turbulence *Physics-Uspekhi*, **43**, 863.
- Danilov, G. and Gurarie, D. 2001a Forced two-dimensional turbulence in spectral and physical space *Phys. Rev. E*, **63**, 061208.
- Danilov, G. and Gurarie, D. 2001b Nonuniversal features of forced twodimensional turbulence in the energy range *Phys. Rev. E*, **63**, 020203-1.
- Danilov, S. and Gurarie, D. 2004 Scaling, spectra and zonal jets in beta-plane turbulence *Phys. Fluids*, **16**, 2592.
- DRITSCHEL, D. G. 1995 A general theory for two-dimensional vortex interactions J. Fluid Mech., **293**, 269.
- DRITSCHEL, D. G., TRAN, C. V. AND SCOTT, R. 2007 Revisiting Batchelor's theory of two-dimensional turbulence *J. Fluid Mech.*, **591**, 379.
- Falkovich, G. 1994 Bottleneck phenomenon in developed turbulence *Phys. Fluids*, **6**, 1411.

- GAGE, K. S. AND NASTROM, G. D. 1986 Theoretical interpretation of atmospheric wave number spectra of wind and temperature observed by commercial aircraft during GASP J. Atm. Sci., 43, 729.
- GILBERT, A. D. 1988 Spiral structures and spectra in two-dimensional turbulence J. Fluid Mech., 193, 475.
- VON HARDENBERG, J., MCWILLIAMS, J. C., PROVENZALE, A., SHCHEPETKIN, A. AND WEISS, J. B. 2000 Vortex merging in quasi-geostrophic flows *J. Fluid Mech.*, **412**, 331.
- HOLTON, J. R. 2004 An introduction to dynamic meteorology: 4th edition *Elsevier Academic Press*.
- Hua, B. L. and Haidvogel, D. B. 1986 Numerical simulations of the vertical structure of quasi-geostrophic turbulence J. Atm. Sci., 43, 2923.
- Kaneda, Y. and Ishihara, T. 2001 Nonuniversal k^{-3} energy spectrum in stationary two-dimensional homogeneous turbulence *Phys. Fluids*, **13**, 1431.
- Kraichnan, R. H. 1967 Inertial ranges in two-dimensional turbulence *Phys. Fluids*, **10**, 1417.
- Kraichnan, R. H. 1971 Inertial-range transfer in two- and three-dimensional turbulence J. Fluid Mech., 47, 525.
- Kraichnan, R. H. 1974 On Kolmogorov's inertial-range theories J. Fluid Mech., 62, 305
- Kukharkin, N. and Orszag, S. A. 1996 Generation and structure of Rossby vortices in rotating fluids *Phys. Rev. E*, **54**, 4524.
- Landau, L. D. and Lifshitz, E. M. 1987 Fluid Mechanics, Second edition *Pergamon Press*, **6** 140.
- Legras, B., Santangelo, P., and Benzi, R. 1988 High-resolution numerical experiments for forced two-dimensional turbulence *Europhys. Lett.*, 5, 37.
- LEITH, C. E. 1968 Diffusion approximation for two-dimensional turbulence *Phys. Fluids*, **11**, 671.
- LILLY, D. K. 1983 Stratified turbulence and the mesoscale variability of the atmosphere J. Atm. Sci., 40, 749.
- LINDBORG, E. 1999 Can the atmospheric kinetic energy spectrum be explained by two-dimensional turbulence? *J. Fluid Mech.*, **388**, 259.
- LINDBORG, E. AND ALVELIUS, K. 2000 The kinetic energy spectrum of the twodimensional enstrophy turbulence cascade *Phys. Fluids*, **12**, 945.
- LINDBORG, E. 2006 The energy cascade in a strongly stratified fluid *J. Fluid Mech.*, **550**, 207.
- MALTRUD, M. E. AND VALLIS, G. K. 1991 Energy spectra and coherent structures in forced two-dimensional and beta-plane turbulence *J. Fluid Mech.*, **228**, 321.
- McWilliams, J. C. 1984 The emergence of isolated coherent vortices in turbulent flow *J. Fluid Mech.*, **146**, 21.
- MCWILLIAMS, J. 1989 Statistical properties of decaying geostrophic turbulence J. Fluid Mech., 198, 199.
- McWilliams, J., Weiss, J. B. and Yavneh, I. 1999 The vortices of homogeneous geostrophic turbulence *J. Fluid Mech.*, **401**, 1.
- Nastrom, G. D. and Gage, K. S. 1985 A climatology of atmospheric wave number spectra of wind and temperature observed by commercial aircraft *J. Atm. Sci.*, **42**, 950.

- Pasquero, C. and Falkovich, G. 2002 Stationary spectrum of vorticity cascade in two-dimensional turbulence *Phys. Rev. E*, **65**, 056305.
- Pedlosky, J. 1987 Geophysical fluid dynamics: 2nd edition Springer-Verlag New York.
- Reinaud, J. N., Dritschel, D. G. and Koudella, C. R. 2003 The shape of vortices in quasi-geostrophic turbulence *J. Fluid Mech.*, **474**, 175.
- RHINES, P. B. 1975 Waves and turbulence on a beta-plane J. Fluid Mech., 69, 417.
- RICHARDSON, L. F. 1922 Weather prediction by numerical process *Cambridge University Press*, Cambridge.
- Scott, R. K. 2007 Nonrobustness of the two-dimensional turbulent inverse cascade *Phys. Rev. E.*, **75**, 046301.
- SMITH, L. M. AND YAKHOT, V. 1994 Finite-size effects in forced two-dimensional turbulence J. Fluid Mech., 274, 115.
- SMITH, K. S. 2004 A local model for planetary atmospheres forced by small-scale convection J. Atm. Sci., 61, 1420.
- Tabeling, P. 2002 Two-dimensional turbulence: a physicist approach *Physics Reports*, **362**, 1.
- Tran, C. V. and Bowman, J. C. 2004 Robustness of the inverse energy cascade in two-dimensional turbulence *Phys. Rev. E.*, **69**, 036303.
- Tung, K. K. and Orlando, W. W. 2003 The k^{-3} and $k^{-5/3}$ energy spectrum of atmospheric turbulence: quasigeostrophic two-level model simulation *J. Atm. Sci.*, **60**, 824.
- Vallis, G. K. and Maltrud, M. E. 1993 Generation of mean flows and jets on a beta plane and over topography *J. Phys. Ocean.*, **23**, 1346.
- Vallis, G. K. 2006 Atmospheric and oceanic fluid dynamics: fundamentals and large-scale circulation *Cambridge University Press*, Cambridge.